Article

Cell Metabolism

Acyl-CoA-Binding Protein Is a Lipogenic Factor that Triggers Food Intake and Obesity

Graphical Abstract

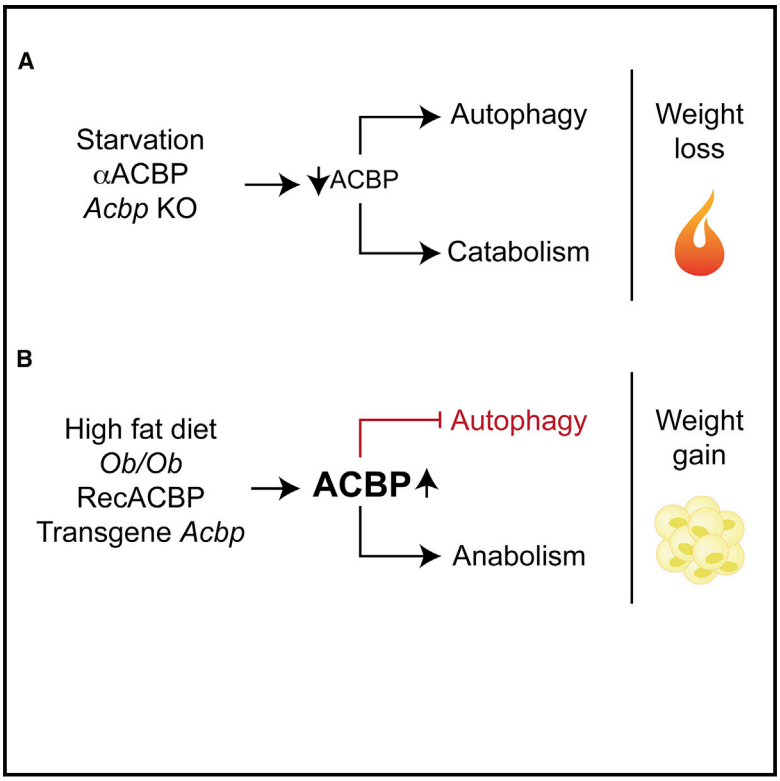

Authors

José M. Bravo-San Pedro, Valentina Sica, Isabelle Martins, ..., Carlos López-Otín, Christophe Magnan, Guido Kroemer

Correspondence

kroemer@orange.fr

In Brief

Bravo-San Pedro et al. investigate the physiological role of the autophagic regulator ACBP, describing that the protein is increased in obese individuals and favors lipogenesis in mouse models, whereas its neutralization reduces the propensity of mice to gain weight in the context of a high-fat diet.

Highlights

- Upon autophagy induction, human and mouse cells release ACBP from the cytoplasm
- ACBP levels are abnormally low in anorexia nervosa patients and elevated in obesity
- Administration of ACBP has lipo-anabolic and obesogenic effects on mice
- ACBP knockout or antibody-mediated neutralization induces lipo-catabolism in mice

Bravo-San Pedro et al., 2019, Cell Metabolism *30*, 754–767
October 1, 2019
https://doi.org/10.1016/j.cmet.2019.07.010

CellPress

CellPress

Cell Metabolism
Article

Acyl-CoA-Binding Protein Is a Lipogenic Factor that Triggers Food Intake and Obesity

José M. Bravo-San Pedro,[1,2,3,27] Valentina Sica,[1,2,3,27] Isabelle Martins,[1,2,3] Jonathan Pol,[1,2,3] Friedemann Loos,[1,2,3] Maria Chiara Maiuri,[1,2,3] Sylvère Durand,[1,2,3] Noélie Bossut,[1,2,3] Fanny Aprahamian,[1,2,3] Gerasimos Anagnostopoulos,[1,2,3,4] Mireia Niso-Santano,[5] Fernando Aranda,[6] Ignacio Ramírez-Pardo,[7] Justine Lallement,[8] Jessica Denom,[8] Erwan Boedec,[9,10,11] Philip Gorwood,[12,13] Nicolas Ramoz,[13] Karine Clément,[14]

(Author list continued on next page)

[1]INSERM U1138, Centre de Recherche des Cordeliers, Sorbonne Université, Université de Paris, Paris, France
[2]Team "Metabolism, Cancer & Immunity", Équipe 11 labellisée par la Ligue contre le Cancer, Paris, France
[3]Metabolomics and Cell Biology Platforms, Gustave Roussy Cancer Campus, Villejuif, France
[4]Faculté de Médecine, Université de Paris Saclay, Kremlin Bicêtre, France
[5]Biomedical Research Networking Center on Neurodegenerative Diseases (CIBERNED), Department of Biochemistry and Molecular Biology and Genetics, University of Extremadura, Faculty of Nursing and Occupational Therapy, Cáceres, Spain
[6]Group of Immune receptors of the Innate and Adaptive System, Institut d'Investigacions Biomédiques August Pi i Sunyer (IDIBAPS), Barcelona, Spain
[7]Department of Cellular and Molecular Biology, Centro de Investigaciones Biológicas, CSIC, Madrid, Spain
[8]Université of Paris, Unité de Biologie Fonctionnelle et Adaptative, CNRS UMR 8251, Paris, France
[9]INSERM U1149, Center of Research on Inflammation, Paris, France
[10]Paris Diderot University, Sorbonne Paris Cité, Paris, France
[11]National French Center of Scientific Research (CNRS), ERL 8252, Paris, France
[12]Clinique des Maladies Mentales et de l'Encéphale (CMME), Hôpital Sainte-Anne, Université of Paris, Paris, France
[13]INSERM U894, Centre de Psychiatrie et Neurosciences (CPN), Université of Paris, Paris, France
[14]Sorbonne Université, Inserm, NutriOMics team, Pitié-Salpêtrière Hospital, Paris, France
[15]University of Lille, CHU Lille, Inserm UMR 1190, European Genomic Institute for Diabetes, Lille, France

(Affiliations continued on next page)

SUMMARY

Autophagy facilitates the adaptation to nutritional stress. Here, we show that short-term starvation of cultured cells or mice caused the autophagy-dependent cellular release of acyl-CoA-binding protein (ACBP, also known as diazepam-binding inhibitor, DBI) and consequent ACBP-mediated feedback inhibition of autophagy. Importantly, ACBP levels were elevated in obese patients and reduced in anorexia nervosa. In mice, systemic injection of ACBP protein inhibited autophagy, induced lipogenesis, reduced glycemia, and stimulated appetite as well as weight gain. We designed three approaches to neutralize ACBP, namely, inducible whole-body knockout, systemic administration of neutralizing antibodies, and induction of antiACBP autoantibodies in mice. ACBP neutralization enhanced autophagy, stimulated fatty acid oxidation, inhibited appetite, reduced weight gain in the context of a high-fat diet or leptin deficiency, and accelerated weight loss in response to dietary changes. In conclusion, neutralization of ACBP might constitute a strategy for treating obesity and its co-morbidities.

INTRODUCTION

Macroautophagy (in short "autophagy") contributes to the maintenance of cellular and organismal homeostasis by mediating the turnover of dispensable cytoplasmic structures (Levine and Kroemer, 2019). In particular, autophagy facilitates the

Context and Significance

Cells respond to changes in the availability of nutrients, but the effect of their response on the metabolism of the whole body is unclear. In this article, researchers in Paris, France, show that when starved, cells secrete acyl-CoA-binding protein (ACBP). In mice, ACBP promotes the production of lipids, induces appetite, and stimulates weight gain; on the other hand, blocking this protein reduces obesity, diabetes, and fatty liver. In humans, ACBP levels are abnormally low in persons with anorexia nervosa but excessively high in obese patients, suggesting that blocking ACBP may help promote body weight loss and that, on the other hand, its administration may be beneficial in patients with anorexia.

Veronique Pelloux,[14] Alili Rohia,[14] François Pattou,[15] Violeta Raverdy,[15] Robert Caiazzo,[15] Raphaël G.P. Denis,[8] Patricia Boya,[7] Lorenzo Galluzzi,[2,16,17,18] Frank Madeo,[19,20] Stéphanie Migrenne-Li,[8] Céline Cruciani-Guglielmacci,[8] Nektarios Tavernarakis,[21,22] Carlos López-Otín,[1,23] Christophe Magnan,[8] and Guido Kroemer[1,2,3,24,25,26,28,*]
[16]Department of Radiation Oncology, Weill Cornell Medical College, New York, NY, USA
[17]Sandra and Edward Meyer Cancer Center, New York, NY, USA
[18]Department of Dermatology, Yale School of Medicine, New Haven, CT, USA
[19]BioTechMed, Graz, Austria
[20]Institute of Molecular Biosciences, NAWI Graz, University of Graz, Humboldtstrasse, Graz, Austria
[21]Department of Basic Sciences, Faculty of Medicine, University of Crete, Heraklion, Crete, Greece
[22]Institute of Molecular Biology and Biotechnology, Foundation for Research and Technology, Hellas, Nikolaou Plastira 100, Heraklion, Crete, Greece
[23]Departamento de Bioquímica y Biología Molecular, Instituto Universitario de Oncología (IUOPA), Universidad de Oviedo, Oviedo, Spain
[24]Pôle de Biologie, Hôpital Européen Georges Pompidou, AP-HP, Paris, France
[25]Suzhou Institute for Systems Medicine, Chinese Academy of Sciences, Suzhou, China
[26]Karolinska Institute, Department of Women's and Children's Health, Karolinska University Hospital, Stockholm, Sweden
[27]These authors contributed equally
[28]Lead Contact
*Correspondence: kroemer@orange.fr
https://doi.org/10.1016/j.cmet.2019.07.010

adaptation to nutritional stress by degrading intracellular macromolecules including proteins, lipids, and glycogen into small molecules that fuel energy metabolism (Galluzzi et al., 2014).

Derangements of autophagy—and in particular its inhibition—play a role in all major human diseases including cancer (Amaravadi et al., 2016), cardiovascular disease (Henning and Brundel, 2017), and neurodegeneration (Menzies et al., 2017), as well as obesity and its co-morbidities (López-Otín et al., 2016). Thus, both genetic and pharmacological inhibition of autophagy compromise weight loss induced by starvation and develop obesity and diabetes (Fernández et al., 2017; He et al., 2013). Circumstantial evidence indicates that obesity is associated with suppressed autophagic flux (Boudoures et al., 2017; Mizunoe et al., 2017; Potes et al., 2017), in line with the fact that its metabolic correlates including hyperglycemia (Roberts et al., 2014), hyperlipidemia (Koga et al., 2010), and hyperinsulinemia (Gulati and Thomas, 2007) actually inhibit autophagy. The etiological link between excessive adiposity and accelerated manifestation of age-associated diseases might involve disabled autophagy (López-Otín et al., 2016).

Although autophagy is mostly studied as a cell-autonomous event, there is evidence that autophagy may affect the communication between cells as well. Thus, autophagy regulates the turnover of cell surface receptors, as exemplified for EGFR (Wei et al., 2013) and cannabinoid receptors (He et al., 2013). Moreover, some factors are released from cells in an autophagy-dependent fashion. This applies to adenosine triphosphate (ATP), the apoptosis-associated release of which depends on the induction of premortem autophagy, with vast consequences for the attraction of myeloid cells into the vicinity of dying cells (Qu et al., 2007; Vacchelli et al., 2015). Moreover, the cellular secretion of several leaderless proteins (which, by definition, can only be released through an unconventional pathway bypassing Golgi) is strongly associated with, and probably depends on, autophagy (Dupont et al., 2011; Ponpuak et al., 2015; Zhang and Schekman, 2013). One such leaderless protein is the phylogenetically ancient factor acyl-CoA-binding protein (ACBP), also known as diazepam-binding protein (DBI) (Duran et al., 2010; Manjithaya et al., 2010). ACBP from human or mouse origin is a small protein of 87 amino acids that has two distinct functions, namely, as ACBP within cells—where it binds to long-chain acyl-CoA molecules, regulating lipid metabolism (Neess et al., 2015)—and as DBI outside cells—where the protein can interact with the benzodiazepine-binding site of the gamma-aminobutyric acid (GABA) type A receptor, $GABA_AR$, and modulate its activity (Bormann, 1991; Christian et al., 2013).

Here, we addressed the question as to whether autophagy-dependent ACBP secretion occurs in mammals and whether ACBP might participate in autophagy regulation and lipid metabolism. We show that ACBP is not only involved in the control of autophagy, but that it also affects general lipid metabolism. This notion is based on the observations that ACBP levels correlate with human body mass index; that increasing ACBP levels in mice triggers lipogenesis, food intake, and weight gain; and that its neutralization increases lipolysis, reduces food intake post-starvation, and causes weight loss in mice.

RESULTS

Autophagy-Dependent Release of ACBP from Human Cells and Mouse Organs

We investigated whether mammalian cells would release ACBP through a similar pathway as yeast (Kinseth et al., 2007). Cells maintained in nutrient-free (NF) condition or treated with rapamycin, two potent stimulators of autophagy, underwent a bona fide autophagic response—as indicated by the lipidation of microtubule-associated protein 1 light chain 3 beta (MAP1LC3B; best known as LC3), the redistribution of a GFP-LC3 fusion protein toward autophagosomes, and the degradation of the autophagy substrate sequestosome 1 (SQSTM1/p62) (Klionsky et al., 2016). This response was accompanied by the depletion of intracellular ACBP detectable by immunoblot analyses of cellular extracts (Figures 1A, 1B, and S1A–S1C), immunofluorescence staining (Figures S1D–S1G), image cytometry (Figures S1H and S1I), or cytofluorimetric analysis (Figures S1J–S1M). The decrease of ACBP protein induced by short-term (4 h) starvation was not accompanied by an equivalent decrease of *ACBP* mRNA (Figure 1C). ACBP decrease was suppressed by the knockdown of the essential autophagy genes *ATG5*, *ATG7*, *ATG10*, or *Beclin 1*; by the addition of lysosomal inhibitors

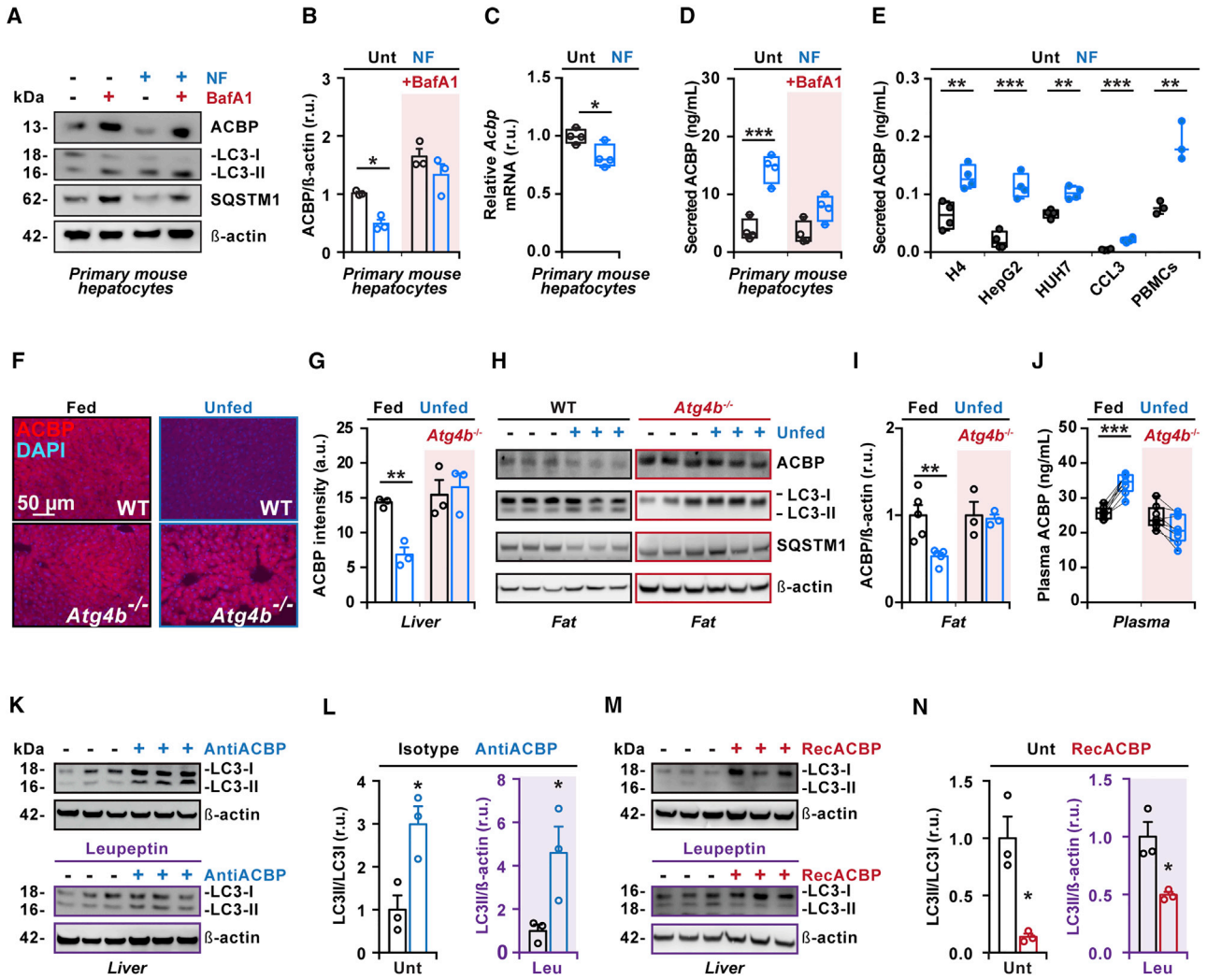

Figure 1. Autophagy-Dependent Release of ACBP

(A and B) Primary mouse hepatocytes were cultured for 4 h in nutrient-free (NF) condition, with or without bafilomycin A1 (BafA1). Representative immunoblots of ACBP, LC3II/I, SQSTM1, and β-actin (A) and densitometric quantification of 3 different experiments (B), upon normalization to the ACBP/β-actin ratio of untreated (Unt) condition.

(C) *Acbp* mRNA expression in primary mouse hepatocytes after 4 h in NF condition (n = 4 mice).

(D and E) ELISA-detectable ACBP in culture media of primary mouse hepatocytes (n = 4 mice per group), human cancer cell lines (D) (n = 4 replicates), and human peripheral blood mononuclear cells (PBMCs) (n = 3 individuals) (E) after the indicated treatments.

(F–J) Autophagy-dependent release of ACBP from mouse organs into the plasma. Representative pictures (F) and quantification (G) of immunofluorescence of ACBP in livers of WT or *Atg4b*$^{-/-}$ mice after 24 h of starvation (unfed). Representative immunoblot (3 representative lanes) (H) and quantification (n = 3 to 5 mice per group) (I) of ACBP levels determined in visceral fat (n = 3 to 5 mice per group). ELISA-detectable ACBP levels in plasma (n = 8 mice per group) (J).

(K–N) Effects of extracellular ACBP on autophagy *in vivo*. Immunoblots and densitometric quantification of LC3 lipidation in liver tissues from mice treated with an ACBP-neutralizing antibody (AntiACBP) (K and L) or recombinant ACBP (RecACBP) (M and N), respectively, with or without the autophagy flux inhibitor leupeptin (leu) (n = 3 mice per group).

Experiments in this figure were performed three times. Results are displayed as box and whisker plots, which show mean, first and third quartiles, and maximum and minimum values (C–E and J) or mean ± SEM (B, G, I, L, and N). For statistical analyses, p values were calculated by two-way ANOVA with Sidak (B, D, G, I, and J) or two-tailed unpaired Student's t test (C, E, L, and N). Symbols indicate statistical comparisons with the control condition (*p < 0.05, **p < 0.01, ***p < 0.001). Open circles (○) indicate values for each mouse and closed circles (•) indicate replicates from *in vitro* experiments. Kilodaltons, kDa; relative units, r.u.; sequestosome, SQSTM1. See also Figures S1–S3.

like bafilomycin A1 (BafA1) and chloroquine; or by inhibiting phosphatidylinositol 3-kinase catalytic subunit type 3 with wortmannin (Figures 1A, 1B, and S1A–S1I). In contrast, ACBP depletion from cells was not inhibited by brefeldin A, an inhibitor of conventional protein secretion, or by the silencing of several genes (STX3, STX4, TRIM10, SNAP29, SNAP23, TRIM16, or SEC22B) involved in the unconventional secretion of interleukin-1β (Kimura et al., 2017) (Figures S1J–S1M). The NF-induced, BafA1-inhibitable release of soluble ACBP into the supernatant could be detected by means of an enzyme-linked

immunosorbent assay (Figures 1D and 1E) or immunoblot (Figure S1C) and did not require *de novo* protein synthesis (Figure S1N). This BafA1-inhibitable ACBP release was observed in primary hepatocytes, peripheral blood mononuclear cells, and multiple human cell lines cultured in NF media (Figures 1D, 1E, S1H, and S1I).

The intracellular levels of ACBP decreased in several organs from autophagy-competent wild-type (WT) mice, but not in *Atg4b*$^{-/-}$ mice (a well-established model of autophagy deficiency) (Mariño et al., 2010), subjected to 24 h of starvation (Figures 1F–1I, S2A, and S2B), a condition that induces autophagy in most tissues from WT mice (Mizushima et al., 2004). In parallel, starvation led to an increase in plasma ACBP levels in WT mice, but not in autophagy-deficient *Atg4b*$^{-/-}$ mice (Figure 1J). Moreover, the starvation-induced surge in plasma ACBP was inhibited by injection of dimethyl α-ketoglutarate and leupeptin (Figure S2C), which suppress the initiation (Mariño et al., 2014) and termination (Esteban-Martinez and Boya, 2015) of autophagy, respectively.

Autophagy-Regulatory Effects of Intracellular and Extracellular ACBP Pools

Intraperitoneal (i.p.) injection of an antibody that neutralizes extracellular ACBP (antiACBP) induced autophagy in the liver (Figures 1K and 1L), while the systemic intravenous (i.v.) administration of recombinant ACBP (recACBP) inhibited autophagy (Figures 1M and 1N). Notably, recACBP enhanced the accumulation of SQSTM1, the phosphorylation of protein kinase B (best known as AKT1), and that of the mechanistic target of rapamycin complex-I (MTORC1) substrate p70^{S6K} in the mouse liver *in vivo* (Figure S2D) and in primary human hepatocytes *in vitro*, together with the phosphorylation of EIF4BP1, another target of MTOR (Figures S2E and S2F). AKT inhibition overcame MTORC1 activation and autophagy inhibition by recACBP (Figure S2F).

Depletion of ACBP by specific small interfering RNAs inhibited NF-driven autophagy and stimulated autophagy-inhibitory MTORC1 activity in human cancer cells *in vitro* (Figures S3A and S3C), while transfection-enforced ACBP overexpression stimulated autophagic flux, as indicated by the redistribution of GFP-LC3 to cytoplasmic puncta, and the lipidation of LC3 (LC3-II) (Figures S3B and S3D). However, when ACBP was depleted (thus autophagy was inhibited) from a majority of human H4 cells that were co-cultured with a minority of ACBP-expressing cells (which are still autophagy-competent), the latter exhibited increased autophagic flux as assessed by measuring GFP-LC3 punctae in the absence or presence of BafA1 (Figures S3E and S3F), confirming the previous *in vivo* results in which we observed that extracellular ACBP inhibits autophagy. Indeed, the addition of antiACBP to cultured human cells stimulated autophagy (Figures S3G and S3H), while the addition of recACBP robustly inhibited NF-driven autophagy (Figures S3I and S3J).

Metabolic Impact of Increasing ACBP Levels

Since extracellular ACBP suppresses autophagy, we investigated whether extracellular ACBP might also affect general metabolism. To this aim, recACBP protein and an antiACBP antibody were injected into fed and starved mice, respectively, and plasma metabolomics were profiled 2 h later. While recACBP reduced glycemia, ACBP neutralization reversed the starvation-induced reduction in blood glucose levels and exacerbated the increase in circulating 2-hydroxybutyric acid (Figure 2A; Table S1). We therefore decided to investigate the effects of ACBP on whole-body metabolism while focusing on energy metabolism.

Increasing ACBP levels, by systemic i.v. injection of recACBP or hydrodynamic injection of plasmids containing a cDNA-ACBP into mice, which caused hepatocyte overexpression of ACBP and increased plasma ACBP levels, stimulated food intake without affecting insulin levels (Figures 2B and S4A–S4D). Accordingly, i.v. injected recACBP rapidly activated orexigenic lateral hypothalamus neurons, as indicated by the nuclear localization of the transcription factor FOS detected by immunohistochemistry (Figures 2C and S4E). Leptin and ghrelin are important endocrine regulators of energy balance and food intake (Farooqi et al., 2001; Inui, 2001). RecACBP injection reduced circulating leptin (Figure S4F) but did not affect ghrelin levels (Figure S4G). Of note, *ob/ob* mice (lacking leptin) showed an increase in circulating ACBP levels in response to starvation (Figure S4H). Moreover, recACBP reduced glucose levels in *ob/ob* mice (Figure S4I), yet failed to further enhance the constitutive hyperphagy of *ob/ob* mice, which was reduced upon leptin injection (Figure S4J). However, injection of a high dose of recombinant leptin (Figure S4K) failed to reverse the drop in glycemia (Figure S4L) and the hyperphagy induced by recACBP injection (Figure S4M), suggesting that ACBP can operate independently from the leptin system. Of note, recACBP injection caused the rapid (within 30 min) increase of liver ACBP levels and glucose transporter solute carrier family 2 member 1 (SLC2A1; best known as GLUT1) and also induced hepatic expression of peroxisome proliferator-activated receptor gamma (PPARG), which stimulates lipogenesis via fatty acid synthase (FASN) transactivation (Figures 2D and S4N). The upregulation of FASN and PPARG in the liver or white adipose tissue (WAT) was observed in starved mice, meaning that it is not secondary to an increased food intake (Figures S4O and S4P). In mice with ad libitum access to food, recACBP reduced fatty acid oxidation, as determined by whole-body respirometry (Figure 2E). Systemic injection of recACBP or transgenic expression of *Acbp* reduced blood glucose levels (Figures 2F and S4Q) and exacerbated the ability of insulin to reduce glycemia in fed mice (Figure S4R), as it enhanced the incorporation of ^{14}C atoms from 2-deoxyglucose into visceral fat (Figure S4S). Mass spectrometric fluxomics with ^{13}C glucose confirmed the increased glucose uptake into adipose tissue upon recACBP injection even in the absence of insulin injection (Figure S4T). The transient drop in blood glucose induced by recACBP injection was abolished by a pharmacological GLUT1 inhibitor (Figure S4U). Importantly, the reversal of the ACBP-induced reduction in glycemia by i.p. injection of glucose (Figure 2G) prevented the increase of food intake (Figure 2H). Thus, ACBP stimulates glucose uptake, which may account for the blood glucose reduction that ultimately drives feeding behavior in mice and reduces the ACBP-mediated activation of orexigenic neurons (Figure S4V).

Effects of ACBP Depletion or Neutralization

To neutralize the extracellular pool of ACBP, we injected mice with suitable monoclonal or polyclonal antiACBP antibodies into the peritoneal cavity. This maneuver reduced food intake post-starvation (Figures 3A and S5A) and increased plasma

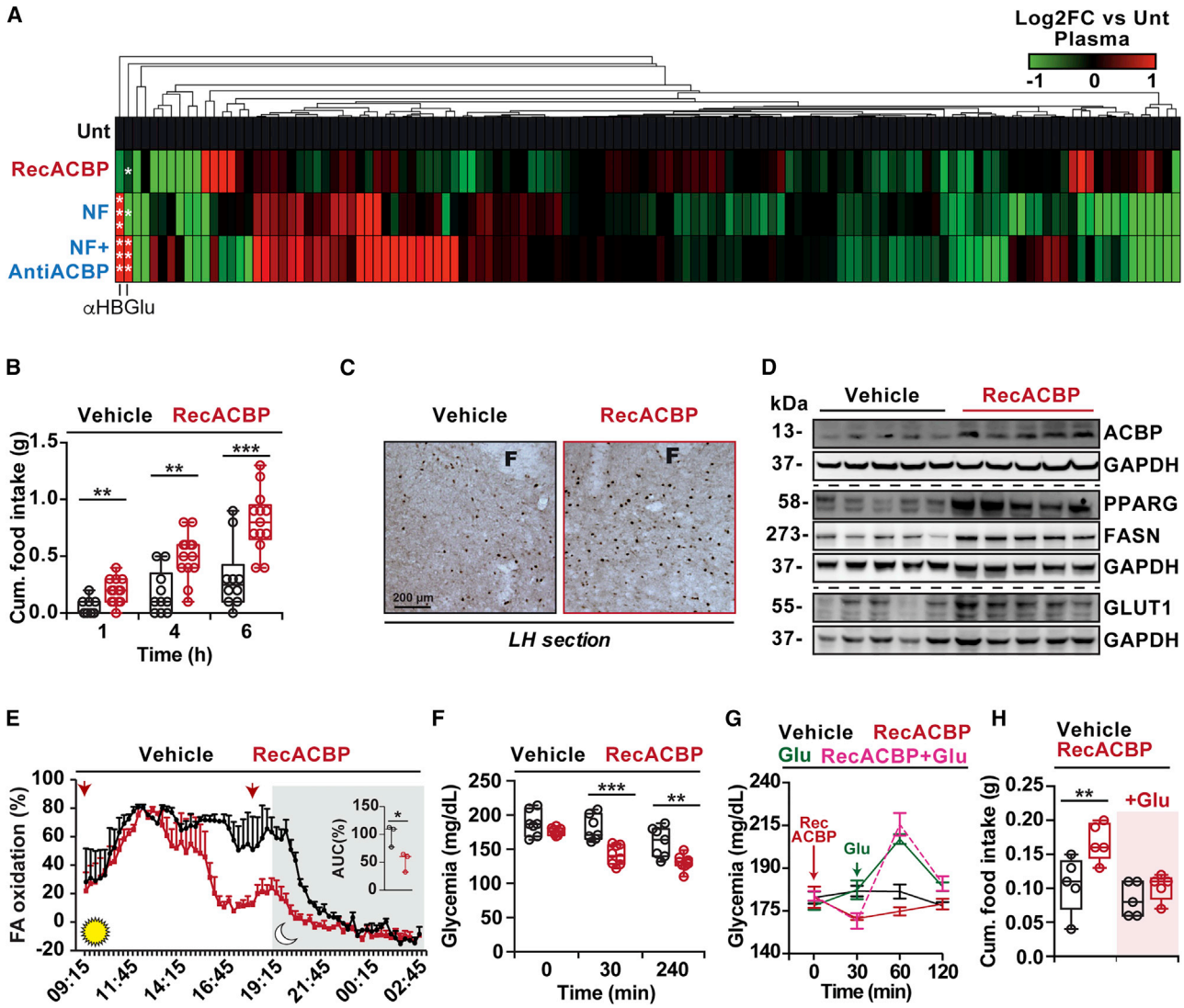

Figure 2. Metabolic Effects of ACBP Increase in Mice

(A) Heatmap clustered by Euclidean distance of changes in liver metabolite concentrations depicted as $\log_2$-fold change (FC) after i.v. recombinant ACBP injection (RecACBP), starvation for 24 h (NF), or NF plus ACBP-neutralizing antibody (antiACBP) in relation to untreated (Unt) mice (n = 3–5 mice per group). The full dataset is reported in Table S1.

(B–H) Metabolic effect of increasing ACBP *in vivo*. (B) Cumulative (cum.) food intake was monitored after recACBP injection (n = 10–13 mice per group). (C) Representative picture of nuclear FOS expression in neurons from lateral hypothalamus (LH) (n = 3 mice per group). (D) Representative immunoblots of ACBP, peroxisome proliferator-activated receptor gamma (PPARG), fatty acid synthase (FASN), glucose transporter solute carrier family 2 member 1 (SLC2A1; best known as GLUT1), and glyceraldehyde-3-phosphate dehydrogenase (GAPDH) in liver tissue (n = 5 mice per group). (E) Fatty acid (FA) oxidation measured by respirometry over 24 h. Area under the curve (AUC) for statistical comparison (n = 3 mice per group). (F) Glycemia after recACBP injection (n = 5–8 mice per group). (G and H) Glycemia (G) and cumulative food intake (H) were monitored during 2 h of recACBP injection in presence or absence of glucose (Glu) (n = 5 mice per group).

Experiments in this figure were performed three times. Results are displayed as heatmap (A) or box and whisker plots, which show mean, first and third quartiles, and maximum and minimum values (B–H). Open circles (○) indicate each mouse used in each experiment. For statistical analysis, p values were calculated by Mann-Whitney U test (A), two-tailed unpaired Student's t test (B, E, and F), or two-way ANOVA with Sidak (H). Symbols indicate statistical comparisons with controls (*$p < 0.05$,**$p < 0.01$,***$p < 0.001$). 2-hydroxybutyric acid, αHB; intravenously, i.v.; fornix, F; grams, g; kilodaltons, kDa. See also Figure S4 and Table S1.

glucose in fed as well as in starved mice (Figures 3B and S5B). ACBP blockade by i.p. injected antibodies rapidly activated neurons in the anorexigenic ventromedial nucleus, and lack of FOS expression was observed in neurons of the orexigenic lateral hypothalamic area (Figures S5C–S5E). ACBP neutralization caused reduction of the hepatic protein levels of ACBP, PPARG, FASN, and the inhibitory phosphorylation of sterol regulatory element-binding transcription factor 1 (SREBF1) (Figures 3C and S5F), and increased plasma adiponectin levels (Figure S5G), suggesting a global activation of lipolysis. Indeed, WAT from antiACBP antibody-injected mice generated more glycerol that WAT from isotype-injected control mice (Figure 3D). AntiACBP injection

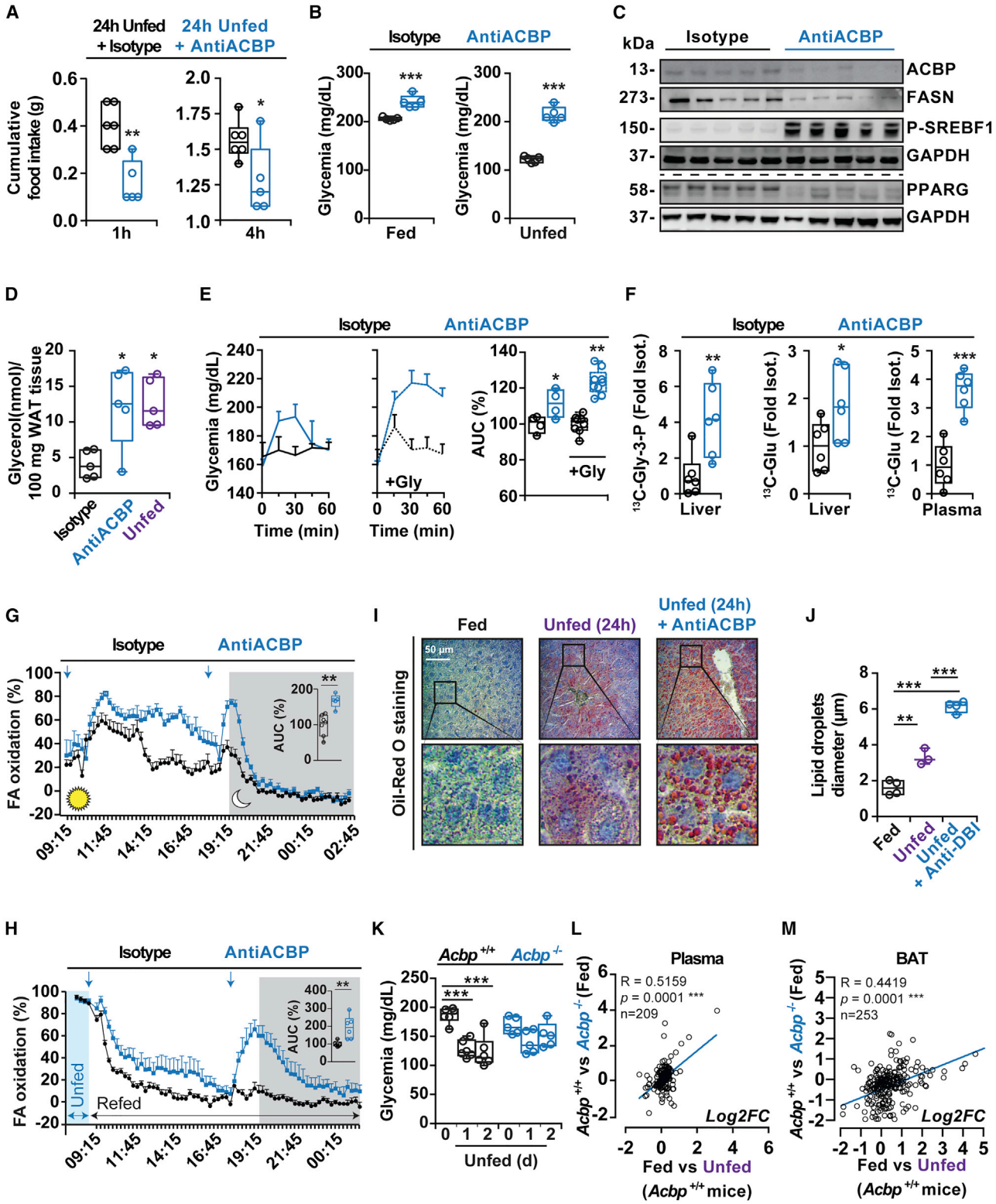

Figure 3. Metabolic Effects of ACBP Neutralization in Mice

(A and B) Cumulative food intake (A) and glycemia (B) were monitored after i.p. antiACBP injection (n = 5 to 6 mice per group).

(C) Immunoblots of ACBP, phospho-sterol regulatory element-binding transcription factor 1 (p-SREBF1), FASN, PPARG, and GAPDH in the liver of mice after antiACBP injection (n = 5 mice per group).

(legend continued on next page)

caused a marked raise in blood glucose levels after glycerol injection (Figure 3E) and a more pronounced conversion of ^{13}C-labeled glycerol into hepatic glycerol-3-phosphate, as well as into glucose in the liver and in the plasma (Figure 3F). ACBP neutralization enhanced whole-body fatty acid oxidation in baseline (Figure 3G) and starved conditions (Figure 3H). Accordingly, ACBP neutralization also augmented the starvation-associated hepatic mobilization of lipids from adipose tissue (Figures 3I and 3J), yet did not prevent hepatic glycogen depletion (Figures S5H and S5I). In spite of the increase in blood glucose induced by ACBP neutralization, starved mice injected with antiACBP exhibited a decrease in plasma insulin, C-peptide, and gastric inhibitory peptide (GIP) levels (Figures S5J–S5L).

Constitutive knockout of *Acbp* in mice results in embryonic death (Landrock et al., 2010) or multiple defects including epidermal barrier dysfunction (Bek et al., 2015), depending on the genetic background. We generated mice in which *Acbp* can be conditionally knocked out by tamoxifen injection (based on the Tam-inducible, Cre recombinase-mediated excision of floxed *Acbp*) (Figures S5M and S5N). In contrast to starved ACBP-expressing controls, ACBP-depleted mice were able to maintain glucose levels in the normoglycemic range (Figure 3K) and circulating ketone bodies were increased after 24 h of starvation (Figure S5O). The metabolomic changes induced by the *Acbp* knockout were very similar to those induced by starvation in normal mice, both in plasma (Figure 3L) and in brown adipose tissue (Figure 3M).

Altogether, these results confirm that ACBP plays a critical role in regulating glucose and lipid metabolism in addition to modulating feeding behavior.

ACBP Levels in Human and Mouse Obesity

In a cohort of 52 patients with anorexia nervosa, plasma ACBP concentrations were lower than in 14 age- and sex-matched controls with a normal body mass index (BMI) (Figure 4A), confirming a prior report on a group of 24 anorexic patients (Conti et al., 2013). More importantly, ACBP concentrations were significantly elevated in obese individuals (Figure 4B), and ACBP levels were reduced along with weight loss 12 months after bariatric-surgery in another group of patients (Figure 4C). Thus, circulating ACBP levels correlated with BMI across several patient subsets (Figure 4D). Elevated ACBP levels in obese individuals correlated with augmented serum insulin (Figure 4E) and aspartate transaminase levels (Figure 4F), which are indicative of (pre-)diabetes and liver dysfunction, respectively. Weight loss upon 6 weeks of hypocaloric regimen (Cotillard et al., 2013) or bariatric intervention led to a temporary reduction of *ACBP* mRNA levels in the periumbilical adipose tissue from obese individuals (Figures 4G and 4H).

Leptin-deficient *ob/ob* mice (which are hyperphagic and become obese even on a normal diet) manifested an increase in *Acbp* mRNA expression and protein levels in liver and adipose tissue (Figures 5A–5D) as well as an increase in circulating ACBP concentrations as compared to their lean controls (Figure 5E). Normal mice rendered obese by a high-fat diet (HFD) also manifested an increase in ACBP protein levels in plasma (Figure 5F), liver, and adipose tissue (Figures 5G and 5H). Conversely, starvation caused a decrease in *Acbp* mRNA (Figures 5I and 5J) and ACBP protein in liver and fat (Figures 1F–1I).

Altogether it appears that a long-term increase in caloric uptake and adiposity, as observed in human obesity, HFD-fed mice, or *ob/ob* mice, is coupled to the transcriptional upregulation of *ACBP* gene expression and a rise in both intracellular and extracellular ACBP protein.

Metabolic Impact of Modifications of ACBP Levels

In the next step, we determined whether manipulation of ACBP would be sufficient to affect body mass. Hydrodynamic injection of plasmids containing a cDNA coding for ACBP into mice caused significant weight gain. This effect was seen with an *Acbp* encoding a strong short-time expression vector, pCMV6, for several days (Figure 5K) as well as with a weaker long-term expression vector, pLIVE, that elevates ACBP levels for several months (Figure 5L). Thus, experimental augmentation of ACBP triggers weight gain. Importantly, the *Acbp* knockout reduced body mass in several conditions. *Acbp* knockout increased weight loss upon starvation (Figure 5M) and attenuated the HFD-induced weight gain (Figure 5N). Moreover, mice that had been rendered obese on an HFD lost more weight when switching to a normal diet that was accompanied by *Acbp* knockout (Figure 5O).

Next, we induced the production of ACBP-neutralizing autoantibodies by repeatedly immunizing mice with ACBP coupled to keyhole limpet hemocyanin (KLH) together with a potent adjuvant (Semerano et al., 2016) (Figures S6A and S6B). Autoimmunization against ACBP leads to enhanced weight loss during starvation (Figure 6A). The weight gain that generally characterizes *ob/ob* mice or WT mice receiving a standard chow or HFD,

(D–F) Lipolysis and gluconeogenesis induced by ACBP neutralization. White adipose tissue (WAT) lipolysis activity, measured as glycerol production (n = 5 mice per group) (D). Gluconeogenic capacity was measured by i.p. glycerol tolerance tests (E) in non-fasted mice. The area under the curve (AUC) was calculated (n = 4 mice per group without glycerol and n = 8 to 9 mice per group with glycerol injection. Mass spectrometry analysis (F) in mice receiving ^{13}C-glycerol (gly) alone or together with antiACBP as the presence of ^{13}C-glycerol-3-P in liver and ^{13}C-glucose (glu) in liver and plasma (n = 6 mice per group).

(G and H) Fatty acid (FA) oxidation measured by respirometry during normal feeding (G) or after 24 h of starvation (Unfed) (H); AUC for statistical comparisons (n = 5 to 7 mice per group).

(I and J) Representative images (I) and quantification of lipid droplet diameters (J) of Oil Red O staining of frozen liver sections from WT mice after 24 h fasting alone or with administration of an ACBP-neutralizing antibody (n = 3 to 4 mice per group).

(K) Glycemia measured in WT (ACBP$^{+/+}$) and ACBP knockout (ACBP$^{-/-}$) mice after 1 or 2 days (d) of fasting (Unfed) (n = 5 to 6 mice per group).

(L and M) Pearson correlations in plasma (L) and brown adipose tissue (BAT) (M) between changes metabolite correlations (Log2FC) after anti-ACBP injection or starvation for 24 h (n = 6 mice per group).

Experiments in this figure were performed three times. Results are displayed as box and whisker plots, which show mean, first and third quartiles, and maximum and minimum values. Open circles (○) indicate each mouse used in each experiment (A–K) or each metabolite analyzed (L and M). For statistical analysis, p values were calculated by two-tailed unpaired Student's t test (A–H), Tukey's multiple comparisons test (J and K), and Pearson's coefficients of correlation (R) (L and M). Symbols indicate statistical comparisons with controls (*p < 0.05, **p < 0.01,***p < 0.001). fornix, F. See also Figure S5.

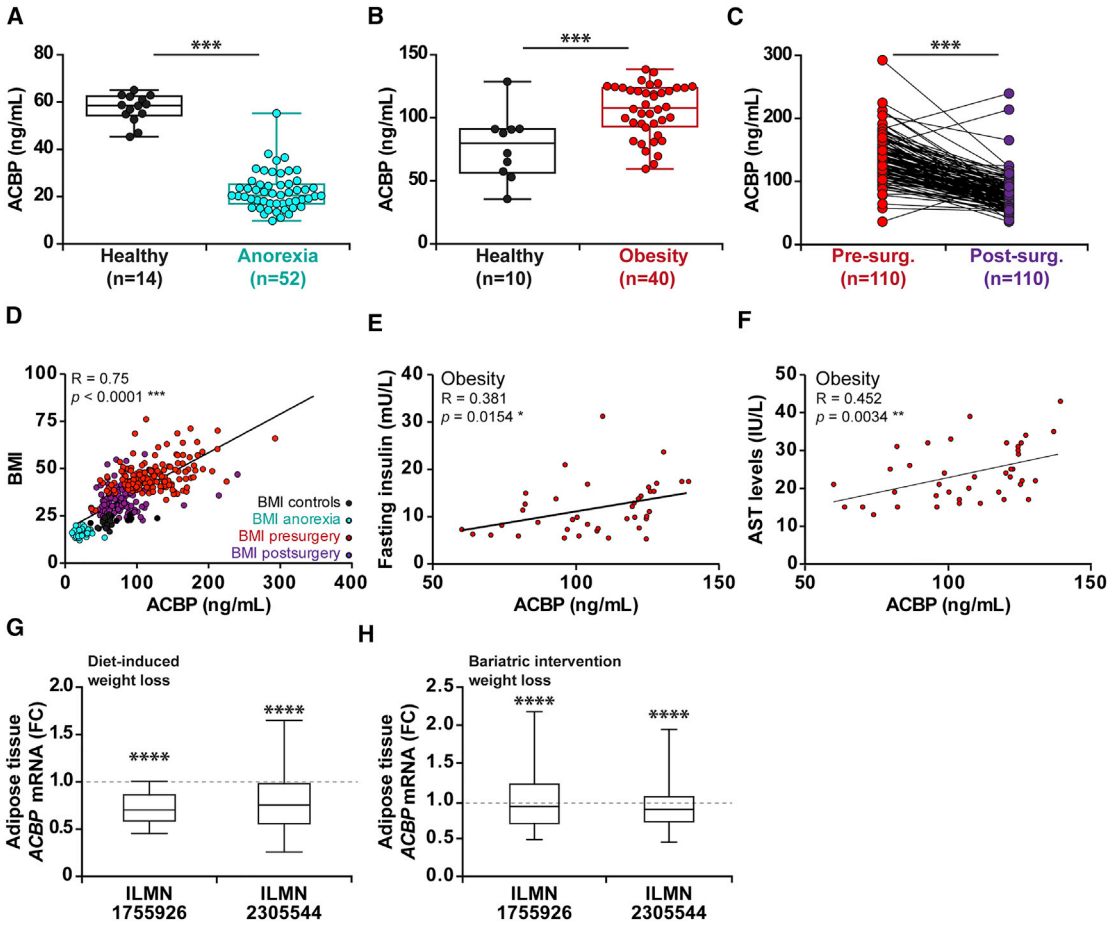

Figure 4. ACBP Levels in Human Anorexia and Obesity

(A–C) Plasma ACBP was measured in cohorts of patients with anorexia nervosa (A, n = 52), obesity (B, n = 40) as compared to age- and sex-matched normal weight controls (A, n = 14; B, n = 10), or in another cohort of obese patients before or 1 year after gastric bypass (C, n = 110).

(D) Correlation between obesity, measured as body mass index (BMI) and plasma ACBP levels in humans (n = 336).

(E and F) Correlation between plasma ACBP levels and circulating insulin in fasting (E) or aspartate transaminase (AST) (F) in obese patients (n = 40).

(G and H) Transient reduction in *ACBP* mRNA levels in adipose tissue from obese patients observing a 6-week-long hypocaloric diet (n = 40) (G) or after bariatric intervention (n = 42) (H). mRNA expression was measured with different oligonucleotide probes (ILMN1755926 and ILMN2305544) and values were normalized to controls.

Results are displayed as box and whisker plots, which show mean, first and third quartiles, and maximum and minimum values. Circles indicate each individual used in each experiment. For statistical analysis, p values were calculated by Mann-Whitney U test (A and B), Wilcoxon matched pairs signed-rank test (C), Pearson's coefficients of correlation (R) (D–F), and false discovery rate (FDR) (G and H). Symbols indicate statistical comparisons with controls (*$p < 0.05$, **$p < 0.01$,***$p < 0.001$,****$p < 0.0001$). Fold change, FC.

respectively, was reduced upon autoimmunization against ACBP (Figures 6B–6E). Coherently, in *ob/ob* mice treated with KLH-ACBP, we observed an increase in carnitine fatty acid esters (and a decrease of phosphatidylcholine) and free fatty acids in plasma (Figures 6F and S6C; Table S2). Moreover, the surge of antiACBP autoantibodies in HFD mice was accompanied by a reduction of absolute fat mass (Figure 6G) and the endogenous mRNA levels of *Acbp* and the lipogenic gene *Pparg* in the liver (Figure 6H). Additionally, HFD-fed mice subjected to ACBP-targeted autoimmunization exhibited less hepatosteatosis (Figures 6I and 6J) and reduced hepatic levels of FASN (Figures S6D and S6F). In the brown adipose tissue (BAT) of HFD-fed mice, the induction of autoantibodies against ACBP was associated with increased uncoupling protein 1 (UCP1) levels, carnitine palmitoyltransferase 1A (CPT-1A, which is required for fatty acid uptake by mitochondria) (Figures S6E and S6G), and total protein content (Figure S6H). Of note, ACBP neutralization also reduced the median size of WAT adipocytes (Figures 6K and 6L), as it normalized the glucose tolerance test in HFD-fed mice (Figure 6M).

DISCUSSION

The unconventional secretion of ACBP has been previously described in yeast (Kinseth et al., 2007) and mammals, more specifically in rabbit glial cells (Qian et al., 2008). However, the underlying mechanisms have remained enigmatic. Here, we provide evidence that autophagy is coupled to the release of intracellular ACBP into the extracellular space in different (non-glial) human cell lines and human peripheral blood

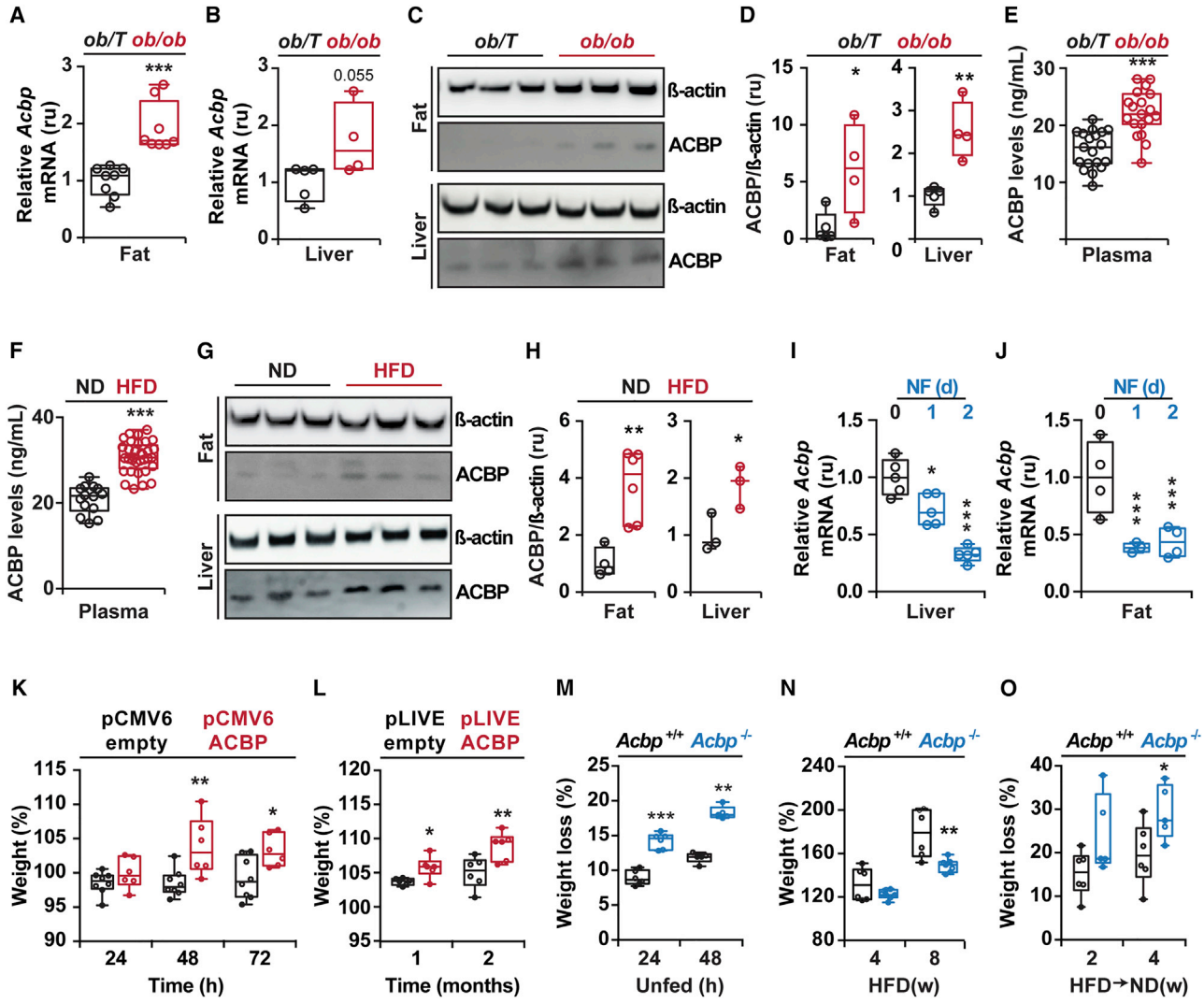

Figure 5. Effect of ACBP on Lipid Metabolism

(A and B) *Acbp* mRNA expression in adipose tissue (fat) (A) and liver (B) from lean mice (*ob/T*) and obese mice (*ob/ob*) (n = 4 to 8 mice per group).

(C and D) Representative immunoblot (n = 3 representative lanes) (C) and densitometric quantification (n = 4 to 5 mice per group) (D) of ACBP/β-actin ratio in liver and fat tissues from *ob/T* and *ob/ob* mice.

(E and F) Plasma ACBP levels from *ob/T* and *ob/ob* mice (n = 19 mice per group) (E) or WT mice feeding normal (ND) or high-fat diet (HFD) (n = 14 to 33 mice per group) (F).

(G and H) Representative immunoblot (n = 3 representative lanes) (G) and densitometric quantification (n = 3 to 6 mice per group) (H) of ACBP/β-actin ratio in liver and fat tissues from WT mice feeding ND or HFD.

(I and J) *Acbp* mRNA expression in liver (n = 5 mice per group) (I) and adipose tissues (n = 4 mice per group) (J) in mice after 1 or 2 days (d) of starvation (NF).

(K and L) Weight measurements after hydrodynamic injection of an ACBP-encoding vector pCMV6 (n = 6 to 8 mice per group) (K) or pLIVE (n = 6 mice per group) (L).

(M–O) Weight measurements of WT ($ACBP^{+/+}$) and ACBP knockout ($ACBP^{-/-}$) mice after 1 or 2 days of starvation (Unfed) (M), HFD feeding (N), and HFD plus switch to normal diet (O) (n = 5 to 8 mice per group).

Experiments in this figure were performed three times. Results are displayed as box and whisker plots, which show mean, first and third quartiles, and maximum and minimum values. Circles indicate each mouse used in the experiment. For statistical analyses, p values were calculated by two-tailed unpaired Student's t test (A–J) or two-way ANOVA with Sidak (K–O). Symbols indicate statistical comparisons with controls mice (*$p < 0.05$, ** $p < 0.01$, ***$p < 0.001$). Hours, h; relative units, ru; weeks, w.

mononuclear cells as well as in several mouse organs. Moreover, we propose a physiological explanation to the link between autophagy induction and the release of ACBP from the intracellular compartment when an energy deficiency occurs.

Of note, we observed a remarkable correlation between ACBP (both intracellular and extracellular levels) and body mass in humans and mice. Thus, in adolescents with anorexia nervosa, the circulating ACBP levels are low, while restrictive dietary interventions in mice decrease intracellular *Acbp* mRNA and ACBP

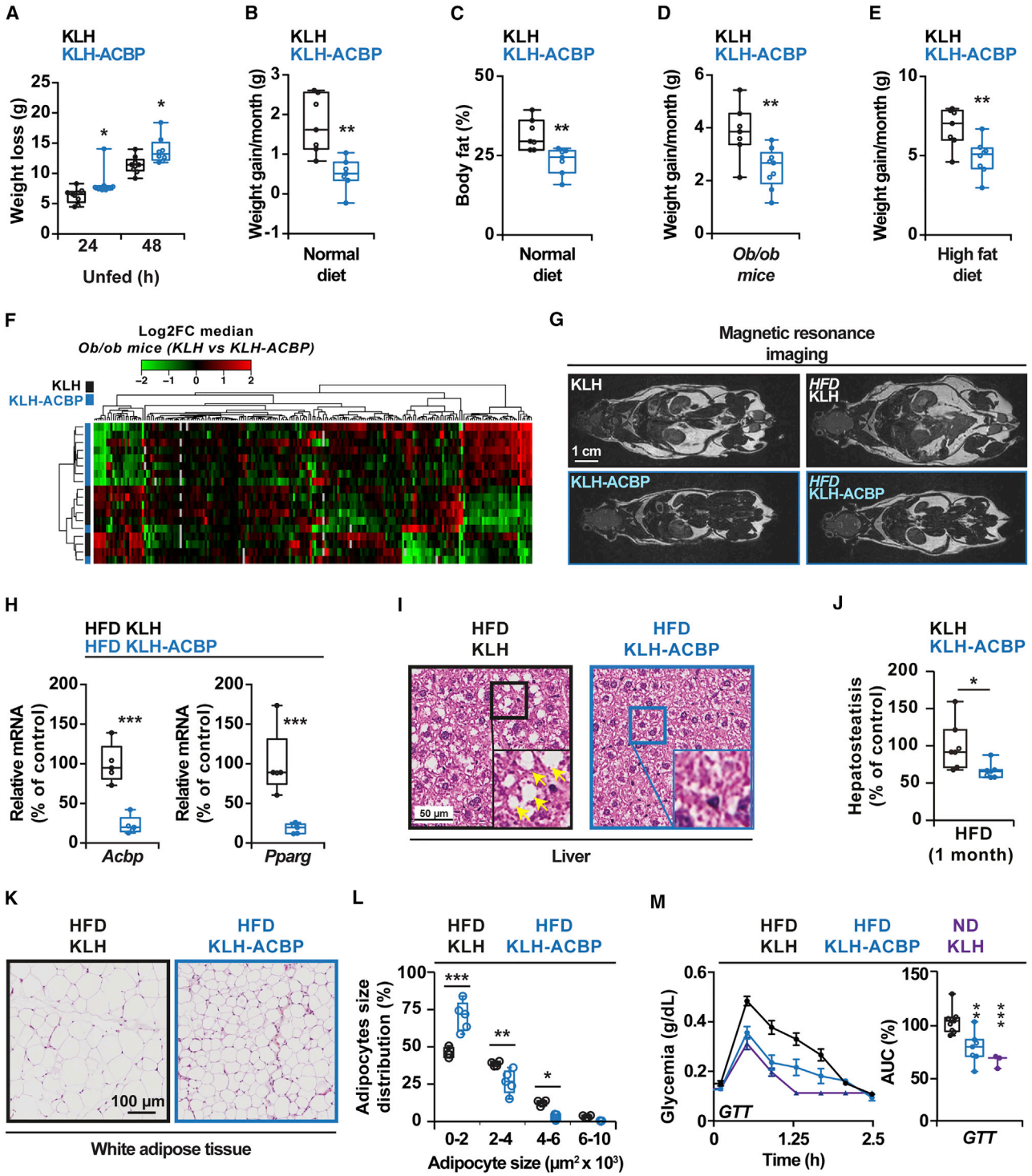

Figure 6. Metabolic Effects of ACBP Neutralization in Mice Undergoing KLH-Based Immunization

(A–E) Weight measurements of mice treated with keyhole limpet hemocyanin (KLH) alone or conjugated to recombinant ACBP (KLH-ACBP) after 1 or 2 days of starvation (Unfed) (n = 8 to 9 mice per group) (A), after a period of normal diet (n = 7 mice per group) (B), or in *ob/ob* mice (n = 7 to 9 mice per group) (D) or high-fat diet (HFD) (E). Percentage of body fat after a period of normal diet was also measured (n = 7 mice per group) (C).

(F) Heatmap clustered by Euclidean distance of changes in plasma metabolite concentrations depicted as $\log_2$ fold change (FC) in obese (*ob/ob*) mice injected with KLH alone or KLH conjugated to recombinant ACBP (KLH-ACBP) (n = 8 to 10 mice per group). See also Figure S6C. The full dataset is reported in Table S2.

(G) Representative images of the whole-body composition analysis of KLH and KLH-ACBP mice after normal diet or HFD.

(H) *Acbp* and *Pparg* mRNA expression in liver from mice vaccinated with KLH or KLH-ACBP and fed with HFD (n = 5 mice per group).

(legend continued on next page)

protein levels in fat and liver tissues. Intriguingly, deletion of *Acbp* or ACBP protein neutralization with endogenous or exogenous antibodies increased autophagy, leading to a parallel dropping of ACBP in the intracellular space and a lipolytic response in mice, enhanced fatty acid oxidation, and stimulated browning of adipose tissue. In turn, these changes generated a temporary hyperglycemia, likewise due to the enhanced conversion of glycerol into glucose, and a consequent anorexic response, which finally limited the weight gain, lipogenesis, adiposity, and hepatosteatosis induced by HFD. Thus, antibody-mediated neutralization of ACBP induced a metabolic response that mimicked that found in conditions of caloric restriction.

Obese patients exhibited elevated plasma levels of ACBP, while a reduction in the *ACBP* mRNA and ACBP plasma protein levels is observed in these patients after an important weight loss. Likewise, obese mice showed an increase in the expression of *Acbp* mRNA and ACBP protein levels in white adipose tissue, liver, and plasma. These results agree with previous findings describing a decrease of ACBP levels in rat liver after 24 h fasting, and augmentations of hepatic ACBP after a 48 h HFD (Bhuiyan et al., 1995). Moreover, ACBP has been reported to favor the differentiation of preadipocytes into adipocytes (Hansen et al., 1991). Obesity is associated with the activation of PPARG (Stienstra et al., 2007), which potently induces lipogenesis and transactivates *ACBP* (Neess et al., 2006). Thus, a long-term increase in body mass may induce an elevation in ACBP by transcriptional upregulation. Of note, murine obesity, whether induced by diet (HFD) or by overeating a normal diet due to leptin deficiency (*ob/ob*), led to similar elevations in *Acbp* mRNA and protein expression. Accordingly, the rise of ACBP levels in mice (resulting from the expression of ACBP-encoding transgenes in hepatocytes or from the injection of recACBP) stimulated a lipogenic response, an increase of glucose uptake into adipose tissue, an increase in food intake, and weight gain. The regulation of food intake and energy metabolism were not depending on leptin, and the orexigenic effect of ACBP seemed to be associated with a temporary reduction in circulating blood glucose levels, as indicated by the fact that glucose injection blunted the ACBP-induced food intake.

Obesity is linked to autophagy inhibition (Boudoures et al., 2017; Mizunoe et al., 2017; Potes et al., 2017), meaning that altered autophagic flux may not explain the augmentation in circulating ACBP but may contribute to the increment of the intracellular ACBP levels. In addition, although we do not know the in-depth role of the extracellular protein, the experiments performed in mice suggest that the obesity-associated rise in plasma ACBP may contribute to autophagy inhibition, which in turn could counteract weight loss and promote weight gain (Fernández et al., 2017; Mariño et al., 2014). Thus, it is possible that extracellular ACBP is part of a feedback regulatory system that self-limits autophagy (Simon et al., 2017).

Our observation that systemic administration of recACBP has orexigenic effects contrasts with prior reports showing that stereotactic or intrathecal administration of proteolytic ACBP fragments into the brain is anxiogenic and anorexigenic (Guillebaud et al., 2017; Lanfray et al., 2013). We believe that several reasons plead in favor of a role for ACBP as a peripheral (rather than central nervous) stimulator of lipo-anabolism and that the modulation of appetite and obesity observed in this work occurs as consequence of ACBP effects on systemic metabolism. First, the hepatic expression of transgenic *ACBP* reduced glucose levels and enhanced food intake. Second, peripherally (i.v.) administered recACBP, which does not cross the blood-brain barrier (Barmack et al., 2004), provoked rapid (within 30 min) metabolic effects leading to enhanced glucose uptake into peripheral tissues, reduced glycemia, and enhanced food intake. Third, the ACBP-induced activation of orexigenic neurons and enhanced feeding was inhibited in conditions of glucose clamp, as a result of the i.p. injection of glucose. Fourth, neutralization of extracellular ACBP by antibodies (which cannot cross the blood-brain barrier) was able to rapidly reduce the activity of orexigenic neurons and activate anorexigenic neurons, again pleading in favor of a peripheral role for ACBP in metabolism and appetite control. Altogether, it appears that ACBP may influence metabolism through systemic effects, independently from its central-nervous impact.

Based on these findings obtained in human and mice, we speculate that, if the long-term blockade of ACBP was exempt of detrimental side effects and constituted a desirable therapeutic goal, autoimmunization against ACBP might be useful for the prevention or treatment of obesity with its co-morbidities.

Limitations of Study

Although the results obtained in mice clearly plead in favor of a role for ACBP in stimulating appetite and obesity, the role of ACBP in human pathophysiology remains to be corroborated by clinical trials. So far, the human data are merely correlative, indicating that ACBP plasma levels are abnormally low in anorexia nervosa and excessively high in obese patients. However, it has to be determined whether an external supply of ACBP may stimulate appetite in anorexic patients. Similarly, the possibility to inhibit ACBP (or its receptor) for controlling excessive appetite and weight gain in obese patients requires further in-depth investigation.

STAR★METHODS

Detailed methods are provided in the online version of this paper and include the following:

- KEY RESOURCES TABLE
- LEAD CONTACT AND MATERIALS AVAILABILITY
  - Materials Availability Statements

(I–L) Histopathological analyses of KLH or KLH-ACBP mice after a period of HFD. Pathological signs of hepatosteatosis (I) and their quantification (J). Representative images of adypocites in KLH and KLH-ACBP treated mice (K) and their size distribution (L) (n = 4 to 7).
(M) Glucose tolerance test (GTT) of mice feeding normal diet (ND) or HFD-induced obese mice immunized with KLH alone or KLH-ACBP. Area under the curve (AUC) for statistical comparison (n = 3 to 9 mice per group).
Experiments in this figure were performed three times. Results are displayed as box and whisker plots, which show mean, first and third quartiles, and maximum and minimum values. Circles indicate each mouse used in the experiment. For statistical analyses, p values were calculated by two-tailed unpaired Student's t test, two-way ANOVA with Sidak (A and L), or Mann-Whitney U test (F). Symbols indicate statistical comparisons with controls KLH immunization or untreated mice (*$p < 0.05$, ** $p < 0.01$, ***$p < 0.001$). Grams, g; hours, h; relative units, ru. See also Figure S6 and Table S2.

SUPPLEMENTAL INFORMATION

Supplemental Information can be found online at https://doi.org/10.1016/j.cmet.2019.07.010.

ACKNOWLEDGMENTS

The authors thank PreclinICAN (Institute of Cardiometabolism and Nutrition, IHU-ICAN, Paris, France) and "Plateforme Imageries du Vivant" INSERM UMR 970 (PARCC-HEGP) for analyses of mouse whole-body composition and Functional & Physiological Exploration Platform (FPE) of the Unit "Biologie Fonctionnelle et Adaptative" (University Paris Diderot, Sorbonne Paris Cité, BFA, UMR 8251 CNRS, Paris, France) for metabolic analyses. The authors thank CRC Core Facilities (CGB, CHIC, and CEF). G.K. is supported by the Ligue Contre le Cancer (équipe labelisée); Agence National de la Recherche (ANR) – projets blancs; Cancéropôle Île-de-France; Chancelerie Des universités de Paris (Legs Poix); the European Research Council (ERC); Inserm Transfert, Fondation Carrefour; Institut National du Cancer (INCa); Inserm (HTE); Institut Universitaire de France; Leducq Foundation; the Labex immuno-Oncology; the RHU Torino Lumière; the Seattle Foundation; and the SIRICs SOCRATE and CARPEM. C.M. and C.C.-G. are supported by Agence National de la Recherche (ANR-16-CE14-0026, fat4brain proposal); C.L.-O. is supported by "Juan de Madariaga fellowship"; S.B. is supported by the Swedish Research Council Vetenskapsrådet (2015-05468) and the Austrian Science Fund FWF (P27183-B24); and F.M. is supported by the Austrian Science Fund FWF (grants P23490-B20, P29262, P24381, P29203, and P27893), DKplus Metabolic and Cardiovascular Diseases (W1226), Austrian Science Ministry, Karl Franzens University ("Unkonventionelle Forschung" and "flysleep"), NAWI Graz, and BioTechMed-Graz flagship project "EPIAge." K.C. is supported by ANR MICRO-Obes and AP/HP (PHRC Microbaria). L.G. is supported by an intramural startup from the Department of Radiation Oncology of Weill Cornell Medical College (New York, US) and by Sotio a.c. (Prague, Czech Republic).

AUTHOR CONTRIBUTIONS

G.K. and J.M.B.-S.P. designed the study and wrote the paper with the help of C.L.-O. J.M.B.-S.P., V.S., I.M., J.P., F.L., G.A., M.C.M., M.N.-S., F.A., I.R.-P., P.B., E.B., R.G.D., J.L., J.D., S.M.-L., and C.C.-G. performed mammalian cell biology and mouse studies. S.D., N.B., and F.A. performed metabolomics analyses. F.M. and N.T. provided phylogenetic insights. P.G., N.R., K.C., A.R., V.P., F.P., R.C., and V.R. provided patient samples and information on the cohorts. K.C., A.R., and V.P. provided the analysis of transient reduction in *ACBP* mRNA levels in adipose tissue from obese patients. C.L.-O., L.G., and M.C.M. provided intellectual input and edited the paper. All authors reviewed the results, edited, and approved the final version of the manuscript.

DECLARATION OF INTERESTS

J.M.B.-S.P. and G.K. filed a patent application dealing with targeting the ACBP/DBI system in anorexia, obesity, and co-morbities. G.K. filed additional patent applications dealing with caloric restriction mimetics (autophagy inducers) for the treatment of aging, age-related diseases, cancer, obesity, and co-morbidities. G.K. is a scientific co-founder of Samsara Therapeutics and Therafast Bio.

Received: February 4, 2019
Revised: June 26, 2019
Accepted: July 19, 2019
Published: August 15, 2019; corrected online: October 25, 2019

REFERENCES

Amaravadi, R., Kimmelman, A.C., and White, E. (2016). Recent insights into the function of autophagy in cancer. Genes Dev. *30*, 1913–1930.

Barmack, N.H., Bilderback, T.R., Liu, H., Qian, Z., and Yakhnitsa, V. (2004). Activity-dependent expression of acyl-coenzyme A-binding protein in retinal Muller glial cells evoked by optokinetic stimulation. J. Neurosci. *24*, 1023–1033.

Bek, S., Neess, D., Dixen, K., Bloksgaard, M., Marcher, A.B., Chemnitz, J., Færgeman, N.J., and Mandrup, S. (2015). Compromised epidermal barrier stimulates harderian gland activity and hypertrophy in ACBP-/- mice. J. Lipid Res. *56*, 1738–1746.

Bhuiyan, J., Pritchard, P.H., Pande, S.V., and Seccombe, D.W. (1995). Effects of high-fat diet and fasting on levels of acyl-coenzyme A binding protein in liver, kidney, and heart of rat. Metabolism *44*, 1185–1189.

Bormann, J. (1991). Electrophysiological characterization of diazepam binding inhibitor (DBI) on GABAA receptors. Neuropharmacology *30*, 1387–1389.

Boudoures, A.L., Saben, J., Drury, A., Scheaffer, S., Modi, Z., Zhang, W., and Moley, K.H. (2017). Obesity-exposed oocytes accumulate and transmit damaged mitochondria due to an inability to activate mitophagy. Dev. Biol. *426*, 126–138.

Bravo-San Pedro, J.M., Pietrocola, F., Sica, V., Izzo, V., Sauvat, A., Kepp, O., Maiuri, M.C., Kroemer, G., and Galluzzi, L. (2017). High-throughput quantification of GFP-LC3^{+} dots by automated fluorescence microscopy. Methods Enzymol *587*, 71–86.

Christian, C.A., Herbert, A.G., Holt, R.L., Peng, K., Sherwood, K.D., Pangratz-Fuehrer, S., Rudolph, U., and Huguenard, J.R. (2013). Endogenous positive allosteric modulation of GABA(A) receptors by diazepam binding inhibitor. Neuron *78*, 1063–1074.

Conti, E., Tremolizzo, L., Bomba, M., Uccellini, O., Rossi, M.S., Raggi, M.E., Neri, F., Ferrarese, C., and Nacinovich, R. (2013). Reduced fasting plasma levels of diazepam-binding inhibitor in adolescents with anorexia nervosa. Int. J. Eat. Disord. *46*, 626–629.

Cotillard, A., Kennedy, S.P., Kong, L.C., Prifti, E., Pons, N., Le Chatelier, E., Almeida, M., Quinquis, B., Levenez, F., Galleron, N., et al. (2013). Dietary intervention impact on gut microbial gene richness. Nature *500*, 585–588.

Dupont, N., Jiang, S., Pilli, M., Ornatowski, W., Bhattacharya, D., and Deretic, V. (2011). Autophagy-based unconventional secretory pathway for extracellular delivery of IL-1beta. EMBO J. *30*, 4701–4711.

Duran, J.M., Anjard, C., Stefan, C., Loomis, W.F., and Malhotra, V. (2010). Unconventional secretion of Acb1 is mediated by autophagosomes. J. Cell Biol. *188*, 527–536.

Esteban-Martínez, L., and Boya, P. (2015). Autophagic flux determination in vivo and ex vivo. Methods *75*, 79–86.

Farooqi, I.S., Keogh, J.M., Kamath, S., Jones, S., Gibson, W.T., Trussell, R., Jebb, S.A., Lip, G.Y., and O'Rahilly, S. (2001). Partial leptin deficiency and human adiposity. Nature *414*, 34–35.

Fernández, Á.F., Bárcena, C., Martínez-García, G.G., Tamargo-Gómez, I., Suárez, M.F., Pietrocola, F., Castoldi, F., Esteban, L., Sierra-Filardi, E., Boya, P., et al. (2017). Autophagy couteracts weight gain, lipotoxicity and pancreatic beta-cell death upon hypercaloric pro-diabetic regimens. Cell Death Dis. *8*, e2970.

Galluzzi, L., Pietrocola, F., Levine, B., and Kroemer, G. (2014). Metabolic control of autophagy. Cell *159*, 1263–1276.

Guillebaud, F., Girardet, C., Abysique, A., Gaigé, S., Barbouche, R., Verneuil, J., Jean, A., Leprince, J., Tonon, M.C., Dallaporta, M., et al. (2017). Glial endozepines inhibit feeding-related autonomic functions by acting at the brainstem level. Front. Neurosci. *11*, 308.

Gulati, P., and Thomas, G. (2007). Nutrient sensing in the mTOR/S6K1 signalling pathway. Biochem. Soc. Trans. *35*, 236–238.

Hansen, H.O., Andreasen, P.H., Mandrup, S., Kristiansen, K., and Knudsen, J. (1991). Induction of acyl-CoA-binding protein and its mRNA in 3T3-L1 cells by insulin during preadipocyte-to-adipocyte differentiation. Biochem. J. *277*, 341–344.

He, C., Wei, Y., Sun, K., Li, B., Dong, X., Zou, Z., Liu, Y., Kinch, L.N., Khan, S., Sinha, S., et al. (2013). Beclin 2 functions in autophagy, degradation of G protein-coupled receptors, and metabolism. Cell *154*, 1085–1099.

Henning, R.H., and Brundel, B.J.J.M. (2017). Proteostasis in cardiac health and disease. Nat. Rev. Cardiol. *14*, 637–653.

Inui, A. (2001). Ghrelin: an orexigenic and somatotrophic signal from the stomach. Nat. Rev. Neurosci. *2*, 551–560.

Izzo, V., Pietrocola, F., Sica, V., Durand, S., Lachkar, S., Enot, D., Bravo-San Pedro, J.M., Chery, A., Esposito, S., Raia, V., et al. (2017). Metabolic interactions between cysteamine and epigallocatechin gallate. Cell Cycle *16*, 271–279.

Kimura, T., Jia, J., Kumar, S., Choi, S.W., Gu, Y., Mudd, M., Dupont, N., Jiang, S., Peters, R., Farzam, F., et al. (2017). Dedicated SNAREs and specialized TRIM cargo receptors mediate secretory autophagy. EMBO J. *36*, 42–60.

Kinseth, M.A., Anjard, C., Fuller, D., Guizzunti, G., Loomis, W.F., and Malhotra, V. (2007). The Golgi-associated protein GRASP is required for unconventional protein secretion during development. Cell *130*, 524–534.

Klionsky, D.J., Abdelmohsen, K., Abe, A., Abedin, M.J., Abeliovich, H., Acevedo Arozena, A., Adachi, H., Adams, C.M., Adams, P.D., Adeli, K., et al. (2016). Guidelines for the use and interpretation of assays for monitoring autophagy, [Third edition]. Autophagy *12*, 1–222.

Koga, H., Kaushik, S., and Cuervo, A.M. (2010). Altered lipid content inhibits autophagic vesicular fusion. FASEB J. *24*, 3052–3065.

Landrock, D., Atshaves, B.P., McIntosh, A.L., Landrock, K.K., Schroeder, F., and Kier, A.B. (2010). Acyl-CoA binding protein gene ablation induces pre-implantation embryonic lethality in mice. Lipids *45*, 567–580.

Lanfray, D., Arthaud, S., Ouellet, J., Compère, V., Do Rego, J.L., Leprince, J., Lefranc, B., Castel, H., Bouchard, C., Monge-Roffarello, B., et al. (2013). Gliotransmission and brain glucose sensing: critical role of endozepines. Diabetes *62*, 801–810.

Lassailly, G., Caiazzo, R., Buob, D., Pigeyre, M., Verkindt, H., Labreuche, J., Raverdy, V., Leteurtre, E., Dharancy, S., Louvet, A., et al. (2015). Bariatric surgery reduces features of nonalcoholic steatohepatitis in morbidly obese patients. Gastroenterology *149*, 379–388.

Levine, B., and Kroemer, G. (2019). Biological functions of autophagy genes: a disease perspective. Cell *176*, 11–42.

López-Otín, C., Galluzzi, L., Freije, J.M.P., Madeo, F., and Kroemer, G. (2016). Metabolic control of longevity. Cell *166*, 802–821.

Manjithaya, R., Anjard, C., Loomis, W.F., and Subramani, S. (2010). Unconventional secretion of pichia pastoris Acb1 is dependent on GRASP protein, peroxisomal functions, and autophagosome formation. J. Cell Biol. *188*, 537–546.

Mariño, G., Fernández, A.F., Cabrera, S., Lundberg, Y.W., Cabanillas, R., Rodríguez, F., Salvador-Montoliu, N., Vega, J.A., Germanà, A., Fueyo, A., et al. (2010). Autophagy is essential for mouse sense of balance. J. Clin. Invest. *120*, 2331–2344.

Mariño, G., Pietrocola, F., Eisenberg, T., Kong, Y., Malik, S.A., Andryushkova, A., Schroeder, S., Pendl, T., Harger, A., Niso-Santano, M., et al. (2014). Regulation of autophagy by cytosolic acetyl-coenzyme A. Mol. Cell *53*, 710–725.

Menzies, F.M., Fleming, A., Caricasole, A., Bento, C.F., Andrews, S.P., Ashkenazi, A., Füllgrabe, J., Jackson, A., Jimenez Sanchez, M., Karabiyik, C., et al. (2017). Autophagy and neurodegeneration: pathogenic mechanisms and therapeutic opportunities. Neuron *93*, 1015–1034.

Mizunoe, Y., Sudo, Y., Okita, N., Hiraoka, H., Mikami, K., Narahara, T., Negishi, A., Yoshida, M., Higashibata, R., Watanabe, S., et al. (2017). Involvement of lysosomal dysfunction in autophagosome accumulation and early pathologies in adipose tissue of obese mice. Autophagy *13*, 642–653.

Mizushima, N., Yamamoto, A., Matsui, M., Yoshimori, T., and Ohsumi, Y. (2004). In vivo analysis of autophagy in response to nutrient starvation using transgenic mice expressing a fluorescent autophagosome marker. Mol. Biol. Cell *15*, 1101–1111.

Neess, D., Kiilerich, P., Sandberg, M.B., Helledie, T., Nielsen, R., and Mandrup, S. (2006). ACBP–a PPAR and SREBP modulated housekeeping gene. Mol. Cell. Biochem. *284*, 149–157.

Neess, D., Bek, S., Engelsby, H., Gallego, S.F., and Færgeman, N.J. (2015). Long-chain acyl-CoA esters in metabolism and signaling: role of acyl-CoA binding proteins. Prog. Lipid Res. *59*, 1–25.

Ponpuak, M., Mandell, M.A., Kimura, T., Chauhan, S., Cleyrat, C., and Deretic, V. (2015). Secretory autophagy. Curr. Opin. Cell Biol. *35*, 106–116.

Potes, Y., de Luxán-Delgado, B., Rodriguez-González, S., Guimarães, M.R.M., Solano, J.J., Fernández-Fernández, M., Bermúdez, M., Boga, J.A., Vega-Naredo, I., and Coto-Montes, A. (2017). Overweight in elderly people induces impaired autophagy in skeletal muscle. Free Radic. Biol. Med. *110*, 31–41.

Qian, Z., Bilderback, T.R., and Barmack, N.H. (2008). Acyl coenzyme A-binding protein (ACBP) is phosphorylated and secreted by retinal Muller astrocytes following protein kinase C activation. J. Neurochem. *105*, 1287–1299.

Qu, X., Zou, Z., Sun, Q., Luby-Phelps, K., Cheng, P., Hogan, R.N., Gilpin, C., and Levine, B. (2007). Autophagy gene-dependent clearance of apoptotic cells during embryonic development. Cell *128*, 931–946.

Roberts, D.J., Tan-Sah, V.P., Ding, E.Y., Smith, J.M., and Miyamoto, S. (2014). Hexokinase-II positively regulates glucose starvation-induced autophagy through TORC1 inhibition. Mol. Cell *53*, 521–533.

Sakurai, T., Amemiya, A., Ishii, M., Matsuzaki, I., Chemelli, R.M., Tanaka, H., Williams, S.C., Richardson, J.A., Kozlowski, G.P., Wilson, S., et al. (1998). Orexins and orexin receptors: a family of hypothalamic neuropeptides and G protein-coupled receptors that regulate feeding behavior. Cell *92*, 573–585.

Semerano, L., Duvallet, E., Belmellat, N., Marival, N., Schall, N., Monteil, M., Grouard-Vogel, G., Bernier, E., Lecouvey, M., Hlawaty, H., et al. (2016).

Targeting VEGF-A with a vaccine decreases inflammation and joint destruction in experimental arthritis. Angiogenesis *19*, 39–52.

Simon, H.U., Friis, R., Tait, S.W., and Ryan, K.M. (2017). Retrograde signaling from autophagy modulates stress responses. Sci. Signal. *10*.

Stienstra, R., Duval, C., Müller, M., and Kersten, S. (2007). PPARs, obesity, and inflammation. PPAR Res. *2007*, 95974.

Vacchelli, E., Ma, Y., Baracco, E.E., Sistigu, A., Enot, D.P., Pietrocola, F., Yang, H., Adjemian, S., Chaba, K., Semeraro, M., et al. (2015). Chemotherapy-induced antitumor immunity requires formyl peptide receptor 1. Science *350*, 972–978.

Wei, Y., Zou, Z., Becker, N., Anderson, M., Sumpter, R., Xiao, G., Kinch, L., Koduru, P., Christudass, C.S., Veltri, R.W., et al. (2013). EGFR-mediated Beclin 1 phosphorylation in autophagy suppression, tumor progression, and tumor chemoresistance. Cell *154*, 1269–1284.

Zhang, M., and Schekman, R. (2013). Cell biology. Unconventional secretion, unconventional solutions. Science *340*, 559–561.

STAR★METHODS

KEY RESOURCES TABLE

REAGENT or RESOURCE	SOURCE	IDENTIFIER
Antibodies		
4EBP1	Cell Signaling Technologies	Cat# 9452; RRID: AB_331692
AKT	Cell Signaling Technologies	Cat# 9272; RRID: AB_329827
Alexa Fluor 647 anti-human CD45 Antibody Clone HI30	Biolegend	Cat # 304018; RRID: AB_389336
Anti-Mouse IgG-Peroxidase	Sigma	Cat# A9044; RRID: AB_258431
Anti-Rabbit IgG-Peroxidase	Sigma	Cat# A0545; RRID: AB_257896
c-FOS	Santa Cruz	Cat# sc-52-G; RRID: AB_2629503
CPT-1A	Abcam	Cat# ab128568; RRID: AB_11141632
Diazepam Binding Inhibitor human (polyclonal)	Abcam	Cat# ab16871; RRID: AB_302557
Diazepam Binding Inhibitor human or mouse (FL-87 ; monoclonal)	Santa Cruz	Cat# sc-30190; RRID: AB_2211046
Diazepam Binding Inhibitor human (C-9 ; polyclonal)	Santa Cruz	Cat# sc-376853; RRID: AB_2722761
Diazepam Binding Inhibitor mouse (polyclonal)	Abcam	Cat# ab231910
Diazepam Binding Inhibitor mouse 7a (monoclonal)	Fred Hutch Antibody Technology	Fred Hutch Antibody Technology
FASN	Cell Signaling Technologies	Cat# 3180, clone C20G5; RRID: AB_2100796
GAPDH	Abcam	Cat# ab9484; RRID: AB_307274
GLUT1	Thermo Scientific-Pierce	Cat# PA1-46152; RRID: AB_2302087
MAP1LC3B	Cell Signaling Technologies	Cat# 2775; RRID: AB_915950
MTOR	Cell Signaling Technologies	Cat# 2983; RRID: AB_2105622
$p70^{S6K}$	Cell Signaling Technologies	Cat# 9202; RRID: AB_331676
Phospho-4EBP1 (Thr37/46)	Cell Signaling Technologies	Cat# 2855; RRID: AB_560835
Phospho-AKT (Ser473)	Cell Signaling Technologies	Cat# 9271; RRID: AB_329825
Phospho-MTOR (Ser2448)	Cell Signaling Technologies	Cat# 5536; RRID: AB_10691552
Phospho-$p70^{S6K}$ (Thr389)	Cell Signaling Technologies	Cat# 9206, clone 1A5; RRID: AB_2285392
Phospho-SREBP (Ser372)	Cell Signaling Technologies	Cat# 9874; RRID: AB_10949508
PPARG	Cell Signaling Technologies	Cat# 2443, clone 81B8; RRID: AB_823598
SQSTM1	Abnova	Cat# H00008878-M01, clone 2C11; RRID: AB_437085
ß-actin	Abcam	Cat# ab49900, clone AC-15; RRID: AB_867494
UCP1	Abcam	Cat# ab10983; RRID: AB_2241462
Biological Samples		
Human plasma from anorexia nervosa patients	Samples provided by Prof. Philip Gorwood and Dr. Nicolas Ramoz	Center Psychiatry Et Neurosciences. INSERM UMR 894-Team 1
Human plasma from obese patients	Samples provided by Prof. Karine Clément	Center of Research in Human Nutrition, Pitié-Salpêtrière Hospital, Paris, France. Cotillard et al., 2013
Human plasma from obese patients	Samples provided by Prof. Francois Pattou	ABOS study NCT01129297
Chemicals, Peptides, and Recombinant Proteins		
Acetic acid	Sigma	33209-1L
Amicon Ultra-15, PLHK, membrane Ultracel-PL, 100 kDa	Merck	UFC910024
Bafilomycin A1	Tocris	1334

(*Continued on next page*)

Continued

REAGENT or RESOURCE	SOURCE	IDENTIFIER
Bio-Rad protein assay dye reagent	Bio-Rad	Cat# 5000006
Brefeldin A	Sigma	B6542
Chloroquine	Sigma	C6628
Cycloheximide	Sigma	C4859
Deoxy-D-glucose 2-[1-14C]	Perkin Elmer	NEC495A001MC
Glucose-D U-^{13}C6 99%13C	Eurisotop	CLM-1396
Glycerol	Sigma	G9012
Glycerol-$^{13}C_3$	Sigma	489476
Keyhole limpet haemocyanin (KLH)	Stellar Biotechnologies	N/A
Leupeptin	Calbiochem	108976
Methanol	Sigma	14262-1L
Methyl tert-butylether	Sigma	34498-1L
Montanide	Seppic, Paris, France	Montanide ISA-51vg
N-tert-butyldimethylsilyl-N-methyltrifluoroacetamid	Sigma	394882
O-ethylhydroxylamine hydrochloride	Sigma	43504-1g
Oil Red O solution	Sigma	O1391
Perifosine	Sigma	SML0612
Periodic Acid Schiff (PAS)	Sigma	395B
Ponceau S Solution	Sigma	P7170
Pyridine	Sigma	270970-100ml
QIAzol	QIAGEN	74104
Rapamycin	Tocris	1292
Recombinant human ACBP	Elaborated by Erwan Boedec	The Inflammation Research Center, Paris, France
Recombinant mouse ACBP	Elaborated by Erwan Boedec	The Inflammation Research Center, Paris, France
Recombinant mouse leptin	Thermo Fisher	PMP0013
Tamoxifen Free Base	Sigma	T5648
TaqMan Gene Expression Master Mix	Applied Biosystems	4369514
Tributylamine	Sigma	90781-50ml
Wortmannin	Sigma	W1628
WZB-117	Sigma	SML0621-25MG
Critical Commercial Assays		
ACBP, Human specific, ELISA kit	Abnova	KA0532
ACBP, Mouse specific, ELISA kit	Coger	MBS-2025156-96
Metabolic hormones, mouse, MILLIPLEX MAP	Millipore	#MMHMAG-44K,
Adiponectin, mouse, MILLIPLEX MAP	Merk	#MADPNMAG-70K-01
Ghrelin (Total), Rat/Mouse, ELISA Kit	Merk	EZRGRT-91
INS1, Mouse ELISA KIT	Sigma	RAB0817-1KT
Leptin, Mouse ELISA Kit	Merk	EZML-82K
RNeasy Mini Kit	QIAGEN	79306
Lipolysis (Adipocyte) Kit	Sigma	MAK195
Deposited Data		
Scans of the original western blots before cropping	This paper	http://dx.doi.org/10.17632/7hdptr389m.1

(*Continued on next page*)

Continued

REAGENT or RESOURCE	SOURCE	IDENTIFIER
Experimental Models: Cell Lines		
H4 (wt and GFP-LC3 stable expressing) H4 GFP-LC3 lentivirus (LentiBrite GFP-LC3 Lentiviral Biosensor)	ATCC Merck	HTB-148 17-10193
H4 ATG5$^{-/-}$ Elaborated using Knockout ZFN ATG5	Sigma Aldrich	Knockout ZFN ATG5 (NM_004849)
HepG2 (wt and GFP-LC3 stable expressing) HepG2 GFP-LC3 lentivirus (LentiBrite GFP-LC3 Lentiviral Biosensor)	ATCC Merck	HB-8065 17-10193
HUH7	Cells provided by Dr. Patrick Soussan	N/A
CCL-13	Cells provided by Dr. Patrick Soussan	N/A
Mouse primary hepatocytes (Mouse Heps male plateable)	Fisher Scientific	10890041
Human primary hepatocytes (Human Heps male plateable)	Thermofisher	MCPMS
Experimental Models: Organisms/Strains		
C57BL/6 mice	ENVIGO, Harlan	N/A
Atg4b$^{-/-}$ C57BL/6 mice	Gift of Dr. Carlos Lopez-Otin, University of Oviedo, Spain	N/A
B6.Cg-Lep^{ob}/J *ob/ob* (Obese mice)	Charles River Laboratories International	B6OSIMA08SS
S/B6.V-LEP +/*Ob* (Lean control mice)	Charles River Laboratories International	B6TSIMA08SS
B6.V-Lep *ob/ob* JRj mice (Obese mice)	Janvier labs	SM-OB-M
B6.V-Lep *ob*/+ JRj (Lean control mice)	Janvier labs	SM-OBT-M
B6.Cg-Tg(UBC-cre/ERT2)1Ejb/1J	Charles River Laboratories International	B6.Cg-*Ndor1*$^{Tg(UBC-cre/ERT2)1Ejb}$/1J
Acbp$^{fl/fl}$ mice in which loxP sites flank *Acbp* exon 2	OZgene	N/A
Oligonucleotides		
Human		
ACBP primers: CACTGGGACAGAGGCTGAGTTTGAGAAA GCTGCAGAGGAGGTTAGGCACC	Illumina	ILMN_1755926
ACBP primers: TCACGGGCAAGGCCAAG TGGGATGCCTGGAATGAGCTGAAAGGG ACTTCC	Illumina	ILMN_2305544
ACBP	Thermo Fisher	Hs01554584_m1
GAPDH	Thermo Fisher	Hs03929097_g1
PPARG	Thermo Fisher	Hs01115513_m1
Mice		
Acbp	Thermo Fisher	Mm01286585_g1
Ppia	Thermo Fisher	Mm02342430_g1
Pparg	Thermo Fisher	Mm00440940_m1
Fasn	Thermo Fisher	Mm00662319_m1
(1) ACBP01F, CAAAGACCATCTCCCTA AACTC	Sigma	HA08835970
(2) ACBP02R, TGGATAGGGAGAAAAGT CACCT	Sigma	HA08835971
(3) ACBP03F, GAGCACGTACTCGGATG GAAGC	Sigma	HA08835972

(*Continued on next page*)

Continued		
REAGENT or RESOURCE	SOURCE	IDENTIFIER
(4) ACBP04F, GGCTGAACTCCTGGGTG AAGCA	Sigma	HA08835973
Cre1, AGGTTCGTTCACTCATGGA	Sigma	HA08835974
Cre2, TCGACCAGTTTAGTTACCC	Sigma	HA08835975
Recombinant DNA		
pLIVE, Vector Complete System,	Euromedex	CM161017-12
pCMV6	Cliniscience	PS100011
Software and Algorithms		
Adobe Illustrator CS6	Adobe	Ver 16.0.0
Microsoft Office	Microsoft	Ver 2010
Prism	GraphPad	Ver 6
Image J	N/A	Ver 1.51
R software	(http://www.r-project.org/)	N/A
Image Lab 5.2 Software	(Bio-Rad)	Ver 5.2
Metamorph	Universal Imaging Corp	Ver 6.2r4
Image Lab	BioRad	Ver 5.2
FlowJo	N/A	Ver 10.2
Others		
Accu-Chek Performa (glycemia)	Accu-Chek	4702354
Glucofix ß-ketone sensor	Menarini	45800
High Fat Diet, 60 % of the energy from fat (butter)	Safe Augy	260 HF
StepOnePlus Real-Time PCR System	Applied Biosystems	N/A

LEAD CONTACT AND MATERIALS AVAILABILITY

Further information and requests for resources and reagents should be directed to and will be fulfilled by the Lead Contact, Guido Kroemer (kroemer@orange.fr).

Materials Availability Statements

Plasmids generated in this study will be made available upon reasonable request. These plasmids will be deposited at Addgene. The mouse line was generated by Ozgene and can be purchased from this supplier.

EXPERIMENTAL MODEL AND SUBJECT DETAILS

Chemicals, Cell Lines, Culture Conditions

Unless otherwise indicated, media and supplements for cell culture were purchased from Gibco-Invitrogen (Carlsbad, CA, USA), plasticware from Corning B.V. Life Sciences (Schiphol-Rijk, The Netherlands). All cell lines were cultured at 37 °C under 5% CO_2, in medium containing 10% fetal bovine serum, 100 mg/L sodium pyruvate, 10 mM HEPES buffer, 100 units/mL penicillin G sodium and 100 μg/mL streptomycin sulfate. Cell type-specific culture conditions include: (1) Dulbecco's modified Eagle's medium (DMEM) for human brain neuroglioma H4 cells (from 37-year-old Caucasian male), as well as the GFP-LC3-expressing and *ATG5*$^{-/-}$ derivatives, hepatocyte-derived cellular carcinoma HuH7 cells (from 57-year-old Japanese male) and hepatocyte-like CCL-13 cells (donor unknown); (2) Eagle minimum essential medium (EMEM) supplemented as above plus 2 mM glutamine and 1% non-essential amino acids (NEAA) for human hepatocellular carcinoma HepG2 cells (from 15-year-old Caucasian male), and the GFP-LC3-expressing derivative; (3) Williams' Medium E plus hepatocyte maintenance supplement pack for male mouse and human primary hepatocytes plateable (purchased by Thermo Fisher Scientific). Cells were seeded in 6-, 96- or 384-well plates and grown for 24 h before treatment with 10 μM rapamycin, 50 nM bafilomycin A1, alone or in combination, 1 μg/mL Brefeldin A, 50 nM chloroquine or 50 μM cycloheximide. Nutrient-free (NF) conditions were established by culturing cells in serum-free Earle's balanced salt solution (EBSS).

Neutralization and Exogenous Supply of ACBP

The following antibodies against ACBP were used *in vivo* (5 μg/g BW, intraperitoneally, in 200 μL) or *in vitro* (1–10 μg/mL): sc-30190 (polyclonal rabbit IgG antibody, Santa Cruz Biotechnology, CA, USA), ab231910 (polyclonal rabbit IgG antibody, Abcam, Cambridge,

MA, USA), mAb 7A (Fred Hutch Antibody Technology, Seattle, WA, USA). Recombinant mouse or human ACBP (recACBP, from The Inflammation Research Center, Paris, France) was used *in vivo* at 0.5 mg/Kg body weight (intravenously, in total volumes of 50 μL).

Mouse Experiments and Tissue Processing

Wild-type C57BL/6 mice (Envigo, Gannat, France), B6.Cg-Lepob/J *ob/ob* obese mice, S/B6.V-LEP +/*Ob* lean mice(JAX Mice Strain, Charles River Laboratory, Lentilly, France), B6.V-Lep *ob/ob* JRj obese mice (Janvier Labs, Saint Berthevin, France), B6.V-Lep *ob*/+ JRj (Janvier labs) lean mice, *Atg4b*$^{-/-}$ C57BL/6 mice (gift of Dr. Carlos Lopez-Otin, University of Oviedo, Spain) were bred and maintained according to the FELASA guidelines and local guidelines from the Animal Experimental Ethics Committee (#04447.02, #2315-2015101617138161v1, #8530-2017011216394941v2, #10862-2017080217568517v3, France). Male mice were kept in SPF conditions, in standard housing conditions in a temperature-controlled environment with 12 h light/dark cycles and received normal diet (ND) or high-fat diet (HFD; SAFE, Augy, France) and water *ad libitum*. Mice were subjected to 24 h starvation or were injected intraperitoneally or intravenously and sacrificed 1 h or 6 h later. Tissues were snap-frozen in liquid nitrogen, extracted and homogenized in 2 cycles for 20 s at 5,500 rpm using a Precellys 24 tissue homogenator (Bertin Technologies, Montigny-le-Bretonneux, France) in 20 mM Tris buffer (pH 7.4) containing 150 mM NaCl, 1% Triton X-100, 10 mM EDTA and Complete protease inhibitor cocktail (Roche Applied Science). Tissue extracts were then centrifuged at 12,000 g (4 °C) and supernatants were collected. Protein concentration in supernatants was evaluated by the bicinchoninic acid technique (BCA protein assay kit, Pierce Biotechnology, Rockford, IL, USA). Recombinant mouse leptin (50 μg/Kg BW) was administered by *i.p.* injection. Leupeptine (15 mg/Kg BW) and dimethyl α-ketoglutarate (300 mg/Kg BW) were used *in vivo* by two *i.p.* injection, 12 h and 4 h before the end of the experiment. WZB177 (20 mg/Kg BW) was used *in vivo* at by *i.p.* administration.

Conditional ACBP Mice

B6.Cg-Tg(UBC-cre/ERT2)1Ejb/1J mice were obtained from the Jackson Laboratory (Bar Harbor, ME, USA). *Acbp*$^{fl/fl}$ mice in which loxP sites flank *Acbp* exon 2 were generated by OZgene (Bentley, WA, USA). On breeding, genotype was verified by PCR using genomic DNA isolated from tail biopsies with primer pairs specific for *Cre* and *Acbp*. *Acbp* primers:

(1) ACBP01F, CAAAGACCATCTCCCTAAACTC;
(2) ACBP02R, TGGATAGGGAGAAAAGTCACCT;
(3) ACBP03F, GAGCACGTACTCGGATGGAAGC;
(4) ACBP04F, GGCTGAACTCCTGGGTGAAGCA

PCR conditions: 95 °C (5 min); [95 °C (30 sec), 60 °C (30 sec), 72 °C (45 sec)] x 35 cycles; 72 °C (7 min); 4 °C. *Cre* primers: (1) Cre1, AGGTTCGTTCACTCATGGA; (2) Cre2, TCGACCAGTTTAGTTACCC. PCR conditions: 94 °C (3 min); [94 °C (20 s), 61.5 °C (40 s), 72 °C (3 min)] x 35 cycles; 72 °C (7 min); 4 °C. PCR products were separated by electrophoresis in 2% agarose gels and visualized using ethidium bromide.

Cre recombinase was activated by administration of Tamoxifen (*i.p.* 75mg/KG BW tamoxifen/mouse daily during 5 days). Tamoxifen was diluted in corn oil (90%) + Ethanol (10%) at a concentration of 20 mg/ml and shake overnight at 37°C.

ACBP Immunization

Keyhole limpet haemocyanin (KLH; from Stellar Biotechnologies, Port Hueneme, CA, USA) and mouse recACBP were mixed at a 1:20 molar ratio and adjusted gradually to 0.25% (v/v) glutaraldehyde. The reaction was terminated by addition of a glycine solution. After ultrafiltration using a 100 KDa membrane (Millipore, Billerica, MA, USA), a formaldehyde solution was added to 0.2% (v/v) final concentration. The reaction was quenched by addition of a glycine solution followed by an ultrafiltration with 70 mM phosphate buffer (pH 7.8). Male 6-8 week-old C57BL/6 mice obtained from Envigo, were immunized with intramuscular injection of 30, 30, 10, 10 μg of KLH-ACBP or KLH alone as an emulsion (1:1) with Montanide ISA-51vg (Seppic, Paris, France) on days 0, 7, 14 and 21, respectively.

In Vivo ACBP Expression by Hydrodynamic Injection

Mice were injected intravenously with plasmid cDNA (10 μg) (pCMV6 or pLIVE) in saline (8% of the body weight) via the tail vein. DNA injection was completed in less than 5 s.

ACBP Detection in Cell Cultures and Plasma Samples

ACBP levels in culture supernatants were determined using a specific ELISA kit (KA0532 ACBP (Human) ELISA; from Abnova, Taipei, Taiwan). Mouse plasma was harvested from blood collection tubes by centrifugation at 15,000 rpm for 30 min, and ACBP levels were determined by ELISA (MBS2025156; from MyBioSource, San Diego, CA, USA) as instructed by the manufacturer. Human plasma ACBP levels were measured in three different cohorts of patients, one from anorexia nervosa patients (samples from Hôpital Sainte-Anne, Paris, France) and two from obese patients (samples from Pitié-Salpêtrière Hospital, Paris, France (Cotillard et al., 2013) and Genomic Institute for Diabetes, Lille, France (Lassailly et al., 2015), by means of the KA0532 ACBP (Human) ELISA kit. The subjects of the surgical cohort were participants of the ABOS study (NCT01129297), an ongoing prospective trial for the longitudinal assessment of metabolic outcomes before and after gastric banding, an exclusively restrictive weight loss intervention. The study design has been detailed elsewhere. The institutional review board approved the study protocol and patients provided written

informed consent before enrolment. All patients underwent an extensive preoperative multidisciplinary evaluation according to French recommendations. Clinical and biological features were assessed preoperatively and at 1 year after surgery. Study outcomes were weight, body mass index (BMI). Circulating insulin was measured at baseline.

Peripheral Blood Mononuclear Cells Isolation

To prepare peripheral blood mononuclear cells from healthy male and female volunteers, 500 μm of total blood were diluted in 5 mL red blood cell lysis buffer (BioLegend, 420301) for 10 min at room temperature and cells were washed twice in phosphate-buffered saline (PBS; Thermo Fisher Scientific, 10010023).

Leptin, Ghrelin, Insulin, C-peptide, GIP and Adiponectin Detection in Plasma

Plasma was harvested from blood collection tubes by centrifugation at 15,000 rpm for 30 min, and stored at −80 °C until use. Leptin, ghrelin, insulin, C-peptide, GIP and adiponectin levels were measured using a mouse serum adipokine immunoassay kit following the protocol provided by the manufacturers.

Plasmid Transfection and RNA Interference

ACBP-encoding plasmids were obtained from OriGene (Rockville, MD, USA). Transient plasmid transfections were performed with the AttracteneR reagent (Qiagen, Hilden, Germany), and, unless otherwise indicated, cells were analyzed 24 h after transfection. Cells were cultured in 6- or 96-wells plates and transfected at 50-60% confluence. siRNAs were reverse-transfected with the help of the RNAi MaxTM transfection reagent (Invitrogen, Eugene, USA) in the presence of 100 nM of siRNAs specific for ACBP or SMARTpool siRNAs against STX3, STX4, TRIM10, SNAP29, SNAP23, TRIM16, SEC22B, ATG5, ATG7, ATG10, and BECN1 (Qiagen) for 48-96 h. The cells were treated as described and processed for cytofluormetric analysis to assess ACBP levels, or autophagy detection by fluorescent microscopy or western blot analysis. (Qiagen). A scrambled siRNA (SCR) was used as a control, and siRNA-mediated protein downregulation was controlled by immunoblotting.

Cytofluorimetric Assays

Cells were collected using Accutase (StemPro Accutase Cell Dissociation Reagent, ThermoFisher, ref A1110501) and washed twice with PBS upon fixation with PBS at 2% PFA for 20 min at room temperature. Cells were permeabilized with 0.1% Triton X-100 for 10 min, then washed twice with cold blocking buffer (3% bsa, v/v in PBS), followed by overnight staining with primary antibodies at 4 °C. Cells were washed and incubated with secondary antibody AlexaFluor 647-conjugates in blocking buffer (for 60 min) and washed prior to flow cytometer analysis (MACSQuant cytometer (Miltenyi Biotec, Bergisch Gladbach, Germany)).

Multispectral imaging flow cytometry was performed on an AMNIS ImageStream X Mark II equipped with 375-, 488-, 561-, and 642-nm lasers using the 60x magnification lens. Only Hoechst+ events were recorded. The analysis was done with IDEAS software v6.1. Only focused events were included in the analysis, using the gradient RMS feature of bright field images. Singlets were then gated on aspect ratio vs area of bright field and leukocyte subpopulations were gated on a pictogram indicating the intensity of PTPRC/CD45 staining versus dark field. The intensity of ACBP staining was quantified within the entire cell.

Immunofluorescence

Cells were fixed with 4% paraformaldehyde (PFA) for 15 min at room temperature, and permeabilized with 0.1% Triton X-100 for 10 min. Non-specific binding sites were blocked with 5% bovine serum in PBS, followed by overnight staining with primary antibodies at 4 °C. Cells were stained for the detection of ACBP with sc-30190 (Santa Cruz Biotechnology, CA, USA). Primary antibodies were revealed with appropriate AlexaFluor conjugates (Molecular Probes-Invitrogen, Eugene, Oregon, USA). Nuclei were counterstained with 10 μM Hoechst 33342. Standard and confocal fluorescence microscopy assessments (20X/40X) were performed on an IRE2 microscope (Leica Microsystems, Wetzlar, Germany) equipped with a DC300F camera, an LSM 510 microscope (Carl Zeiss, Jena, Germany) or a Leica SPE confocal microscope (Leica Microsystems). Acquired images were converted to 8-bit binary files, and cytoplasmic ACBP intensity on each image was calculated by ImageJ software (NIH). Each experiment was done at least three times.

Automated Microscopy

Cells stably expressing GFP-LC3 were seeded in 96- or 384-well imaging plates (BD Falcon, Sparks, USA) 24 h before stimulation. Cells were treated with the indicated agents for 4-6 h. Subsequently, cells were fixed with 4% PFA and counterstained with 10 μM Hoechst 33342. Images were acquired using an ImageXpress Micro XLS Widefield High-Content Analysis System operated by the MetaXpress Image Acquisition and Analysis Software (Molecular Devices, Sunnyvale, CA, US). Acquisition was performed by means of a 20X PlanApo objective (Nikon, Tokyo, Japan). Minium 9 views fields per well for 96-well or 384-well plate were acquired. MetaXpress was utilised to segment cells into nuclear area (based on Hoechst 33342 signal). GFP-LC3+ dots number per cell are counted within each cytoplasmic ROI based on differential pixel intensity of GFP-LC3 signal. Autophagy level was measured by counting the numbers of GFP-LC3+ puncta per cell. Images were also acquired using a BD pathway 855 automated microscope (BD Imaging Systems, San José, CA, USA) equipped with a 40X objective (Olympus, Center Valley, USA) coupled to a robotized Twister II plate handler (Caliper Life Sciences, Hopkinton, USA). Images were analyzed for the presence of GFP-LC3 puncta in the cytoplasm by means of the BD Attovision software (BD Imaging Systems). Cell-like objects were segmented and divided into

cytoplasmic and nuclear regions as previously reported (Bravo-San Pedro et al., 2017). Rolling-bar 2x2 and Marr-Hildreth algorithms were used to recognize cytoplasmic GFP-LC3^{+} dots. Statistical analyses were implemented on the R bioinformatic environment (http://www.r-project.org/).

Immunoblotting

For immunoblotting, 25 μg of proteins were separated on 4-12% Bis-Tris acrylamide precast gels (Invitrogen) or 12% Tris-Glycine SDS-PAGE precast gels (Biorad, Hercules, CA, USA) and electrotransferred to Immobilon membranes (Millipore). Membranes were horizontally sliced according to the molecular weight of the protein of interest to allow simultaneous detection within the same experiment. Unspecific binding sites were saturated by incubating membranes for 1 h in 0.05% Tween 20 (v:v in TBS) supplemented with 5% non-fat powdered milk (w:v in TBS), followed by overnight incubation with primary antibodies specific for human ACBP (ab16871, Abcam or sc-376853, Santa Cruz), murine ACBP (ab231910, Abcam), SQSTM1 (#H00008878-M01, clone 2C11, Abnova), MAP1LC3B (#2775, Cell Signaling Technologies), FASN (clone C20G5, #3180, Cell Signaling Technologies), phospho-p70^{S6K} (Thr389) (clone 1A5, #9206, Cell Signaling Technologies), p70^{S6K} (#9202, Cell Signaling Technologies), Phospho-SREBP (Ser372) (#9874, Cell Signaling Technologies), GLUT1 (PA1-46152, Thermo Scientific-Pierce), PPARG (clone 81B8, #2443, Cell Signaling Technologies), CPT-1A (ab128568), AKT1 (Cell Signaling, 9272), Phospho-AKT1 (Cell Signaling, 9271), MTOR (Cell Signaling, 2983), Phospho-MTOR (Cell Signaling, 5536), EIF4EBP1 (Cell Signaling, 9452), Phospho-EIF4EBP1 (Cell Signaling, 2855) or UCP1 (ab10983, Abcam). Revelation was performed with appropriate horseradish peroxidase (HRP)-labeled secondary antibodies (Southern Biotech, Birmingham, USA) plus SuperSignal West Pico chemoluminescent substrate (Thermo Scientific-Pierce). Antibodies specific for glyceraldehyde-3-phosphate dehydrogenase (GAPDH, #ab9484, Abcam) or ß-actin (#Ab49900, clone AC-15, Abcam) were used to control equal loading of lanes.

Metabolomic analysis. Sample preparation Tissue: About 30 mg of tissues for each condition were first weighted and solubilized into 1.5 mL polypropylene microtubes with ceramic beads with 225 μL of MEOH. They were then homogenized three times for 20 s at 5500 rpm using Precellys 24 tissue homogenator (Bertin Technologies, Montigny-le-Bretonneux, France). 750 μL of MTBE were added and the samples were homogenized again three times for 20 s at 5500 rpm. 188 μL of MilliQ water were added in the samples, followed by vortex (4 min) and centrifugation (10 min at 15000 g, 4 °C). 700 μL of the organic upper phase of the supernatant were transferred in microtubes for further analysis, and the lower phase was supplemented with 1 ml of MEOH, followed by vortex (5 min) and centrifugation (2 min at 14000 g). The supernatant was split in two parts: the first 300 μL used for the Gas Chromatography coupled by Mass Spectrometry (GC/MS) experiment in microtubes, the others 700 μL used for the Ultra High Pressure Liquid Chromatography coupled by Mass Spectrometry (UHPLC/MS) experimentations. Concerning the GC-MS aliquots, 250 μl were transferred from the microtubes to an injection vial and evaporated. The dried extract was stored at -80 °C until derivatization and analysis. Concerning the UHPLC-MS aliquots, the collected supernatant was evaporated in microtubes at 40 °C in a pneumatically-assisted concentrator (Techne DB3, Staffordshire, UK). The UHPLC-MS dried extracts were solubilized with 200 μL of MilliQ water. One aliquot of 50 μL was transferred in injection vial for direct analysis, and the 150 μL were aliquoted and kept as backup at -80 °C.

Sample Preparation Plasma (Lithium Heparin)

A volume of 50 μL of plasma were mixed with 225 μL of MEOH into 1.5 mL microtubes, vortexed 5 minutes and centrifugated (10 min at 15000 g, 4°C). 750 μL of MTBE were added and the samples were vortexed 1 min. 188 μL of MilliQ water were added in the samples, followed by vortex (4 minutes) and centrifugation (10 min at 15000 g, 4 °C). 700 μL of the organic upper phase of the supernatant were transferred in microtubes for further analysis, and the lower phase was supplemented with 1 ml of MEOH followed by vortex (5 min) and centrifugation (2 min at 14000 g). The supernatant was split in two parts: the first 300 μL used for the GC/MS experiment in microtubes, the others 700 μL used for the UHPLC/MS experimentations. Concerning the GC-MS aliquots, 250 μl were transferred from the microtubes to an injection vial and evaporated. The dried extract was stored at -80°C until derivatization and analysis. Concerning the UHPLC-MS aliquots, the collected supernatant was evaporated in microtubes at 40°C in a pneumatically-assisted concentrator (Techne DB3, Staffordshire, UK). The UHPLC-MS dried extracts were solubilized with 200 μL of MilliQ water. One aliquot of 50 μL was transferred in injection vial for direct analysis and the 150 μL were aliquoted and kept as backup at -80°C.

Labeling Experiment by Targeted Analysis of Nucleoside Phosphates and Cofactors by ion Pairing Ultra-High Performance Liquid Chromatography (UHPLC) Coupled to a Triple Quadrupole (QQQ) Mass Spectrometer

Targeted analysis was performed on a RRLC 1260 system (Agilent Technologies, Waldbronn, Germany) coupled to a Triple Quadrupole 6410 (Agilent Technologies) equipped with an electrospray source operating in negative mode. The gas temperature was set to 350 °C with a gas flow of 12 L/min. The capillary voltage was set to 3.5 kV. 10 μL of sample were injected on a Column Poroshell PhenylHexyl (100 mm x 2.1 mm particle size 2.7 μm) from Agilent technologies, protected by a guard column XDB-C18 (5 mm × 2.1 mm particle size 1.8 μm) and heated at 40°C by a pelletier oven. The gradient mobile phase consisted of water with 10 mM of TBA and 10 mM AA (phase A) and Methanol with 10 mM of TBA and 10mM AA (phase B). The flow rate was set to 0.2 mL/min, and gradient as follow: initial condition was 98% phase A and 2% phase B, maintained during 1 min. Molecules were then eluted using a gradient from 2% to 70% phase B over 10 min. The column was washed using 95% mobile phase B for 2 min and equilibrated using 2% mobile phase B for 4 min. The autosampler was kept at 4°C. The collision gas was nitrogen. The scan mode used was the MRM for biological samples with the Q1 corresponding to the molecule [M-H]- and with Q3 corresponding to an expected fragment. Peak detection and integration of the isomers were performed using the Agilent Mass Hunter quantitative software (B.07.01).

Labeling Experiment by Targeted Analysis or by Gas Chromatography (GC) Coupled to a Triple Quadrupole (QQQ) Mass Spectrometer

Targeted analysis methods are described in Izzo et al. (2017). Briefly, derivatization of GC aliquot was carried out with 50 μL of O-ethylhydroxylamine hydrochloride stored at room temperature in the dark for 16 h followed by silylation with 80 μL of N-tert-butyldimethylsilyl-N-methyltrifluoroacetamid (MSTBFA) at 40°C for 30 min. The GC-MS/MS method was performed on a 7890B gas chromatography (Agilent Technologies, Waldbronn, Germany) coupled to a triple quadrupole 7000C (Agilent Technologies, Waldbronn, Germany) equipped with an electronic impact source (EI) operating in positive mode. The scan mode used was the MRM for biological samples with the Q1 corresponding to the maximally derivatised molecule and with Q3 corresponding to a typical fragment of silyl group (73 or 147). Peak detection and integration of the isotopomers were performed using the Agilent Mass Hunter quantitative software (B.07.01).

Immunohistochemistry on Brain Tissue

Animals were deeply anesthetized with 80 mg/kg intraperitoneally pentobarbital (Nembutal, Abbott Laboratories, Chicago, IL, USA) and perfused transcardially with 0.1 M phosphate buffer (PB), followed by 4% PFA (in 0.1 M PB). Brains were removed, post-fixed for 2 h in the same fixative, cryoprotected in 20% sucrose (in 0.1 M PB) for 48 h, and snap frozen in CO_2. Coronal sections (20 μm) were cut in a CM 3050 cryostat (Leica). The hypothalamic sections were collected in three separate series and were thaw mounted on SuperFrost Plus microscopic glass slides (Faust, Schaffhausen, Switzerland). After air-drying at room temperature and rehydrating in PBS, sections were incubated in blocking solution for 2 h (1.5% rabbit normal serum plus avidin; from Vector Laboratories, Burlingame, CA, USA). Polyclonal goat antiFOS antibodies (from Santa Cruz) was applied at 1:10000 dilution in the presence of biotin for 48 h at 4 °C. Unbound antibodies were removed by washing in PBS before the sections were incubated with secondary antibodies (biotinylated rabbit-anti-goat, 1:200; from the Vectastain-Elite ABC Kit, Vector Laboratories;) for 2 h at room temperature. After incubation in ABC solution, diaminobenzidene (DAB) was used as a chromogen [0.04% in PBS with 0.02% H_2O_2 and 0.08% $NiCl_2$ (×6 H_2O), 0.01% $CoCl_2$ (×6 H_2O) for color enhancement]. Finally, sections were dehydrated in graded alcohols, cleared in xylenes, and coverslipped with Entellan (Merck, Darmstadt, Germany).

Our estimation of the orexigenic nature of cfos positive neurons as a function of their neuroanatomical location in the lateral hypothalamus (LH) is based on the comparison of images obtained in the study of Sakurai et al. (1998) showing the location of LH orexigenic neurons in the same region as described in our study.Energy expenditure and food intake analysis

Mice were analyzed for energy expenditure (EE), oxygen consumption and carbon dioxide production (RQ = vCO_2/vO_2), and food intake using calorimetry (Labmaster, TSE Systems GmbH, Bad Homburg, Germany). Mice were individually housed and acclimated to the chambers for 48 h before experimental measurements. Data analysis was performed using O_2 consumed (mL/h), CO_2 production (mL/h) and energy expenditure (Kcal/h) subsequently expressed as a function of whole lean body mass (LBM). LBM was acquired using an Echo Medical systems EchoMRI 100 (Whole Body Composition Analyser, EchoMRI, Houston, TX, USA). Fatty acid oxidation rate was calculated using the following equation: Fatty acid oxidation (Kcal/h) = EE (Kcal/h) × (1 − RQ/0.3).

Glucose Uptake Measurements

[1-^{14}C]2-deoxyglucose (2-DG) (#NEC495A001MC, Perkin Elmer) and Glucose-D U-^{13}C6 (CLM-1396, Eurisotop) were used to quantitate tissue glucose uptake *in vivo*. [1-^{14}C]2-DG at 3 μCi was injected intraperitoneally (with or without 0.5 IU/kg insulin). Blood was drawn from the tail vein at different time points (3, 5, 10, 20, 30, 40, 60, 75 and 90 min), and glucose concentrations were measured. Twenty μL of blood contained in a heparinized capillary were added to a 1.5 mL tube containing 100 μL $ZnSO_4$ (0.3 N), followed by 100 μL $Ba(OH)_2$ (0.3 N) to precipitate proteins. At completion of the experiment (time 90 min) the samples were centrifuged at 12,000 g for 3 min and 50 μL of supernatant were move to a counting vial and evaporated in a hood. Dry pellet was resuspended in 500 μL water before cpm assessment. Mice were sacrificed by pentobarbital injection and tissues were processed as follows: each tissue was dissected, cleaned, weighed and transferred to a tube containing 0.5 mL NaOH (1 M), shaken on a thermo-mixer (60° C, 950-1000 rpm) for 1 h, followed by addition of 0.5 mL of HCl (1 M). Two-hundred μL of the homogenate were transferred to tubes containing 0.5 mL $ZnSO_4$ (0.3 N), to which 0.5 mL $Ba(OH)_2$ (0.3 N) were then added. Two-hundred μl of the homogenate were transferred to tubes containing 1 mL perchloric acid (6%). After vortexing and centrifuging samples for 2 min at 13000 g, 400 μL of supernatants were transferred to counting vials and radioactivity was determined. The first series with $ZnSO_4$ and $Ba(OH)_2$ allowed for determining Xcpm (2-DG). The second series with PCA allowed for determining Ycpm (2-DG plus 2-deoxyglucose 6 phosphate, 2-DG6P). Ycpm-Xcpm = 2-DG6P synthesis reflecting cellular 2-DG uptake within the tissue.

Glucose-D U-^{13}C6 (2.5 g/kg BW) was injected *i.p.* (with or without 0.5 μg/g BW of recACBP injected *i.v.*). At completion of the experiment (time 120 min) mice were sacrificed and tissues were collected and processes by the metabolome platform.

Glycerol-Stimulated Glucose Production

Animals were fasted for 2 h and given an intraperitoneal injection of ^{13}C-glycerol labeled (1 g/KG BW). Animals were sacrificed after 1h and liver and plasma were collected. Hepatic glucose production was determined by detection of ^{13}C-glycerol-3-P or ^{13}C-glucose in liver and ^{13}C-glucose in plasma by metabolomics analysis.

Glycerol Tolerance Test

Animals were fasted for 2 h and given an intraperitoneal injection of glycerol (1 g/KG BW). Blood was collected from the lateral vein of the tail prior to and at the indicated times after the injection. Glucose was measured using a precision glucometer (Accu-Chek Performa).

Glucose Tolerance Test

Animals were fasted for 16 h and given an intraperitoneal injection of glucose (2.5 g/KG BW). Blood was collected from the lateral vein of the tail prior to and at the indicated times after the injection. Glucose was measured using a precision glucometer (Accu-Chek Performa).

Measurement of Lipolysis

The isolation of adipocytes from adipose tissue and measurement of lipolysis was realized following the protocol provided by the Sigma (MAK195 Sigma-Aldrich).

Histology

After fixation of liver and white adipose tissues, 4 μm thick paraffin sections were stained with hematoxilin-eosin-saffranin or frozen sections with Oil-Red. Each slide was examined using a Zeiss Axiophot microscope.

Analysis of Whole-Body Composition

Non-invasive determination of lean tissue mass, fat mass and free fluid was performed on non-anesthetized mice using TD-NMR technology (minispec LF90II; Bruker BioSpin) at PreclinICAN. In other experiments, MRI was performed with a dedicated small-animal 4.7 Tesla MR system (Biospec 47/40 USR Bruker) using a quadrature transmit/receive body coil with a 7 cm inner diameter (Plateforme Imageries du Vivant, INSERM UMR 970). Mice were anesthetized with air and isoflurane (4% for induction and 1% during MRI). Experiments were performed with respiratory gating to avoid movement artifact. We used a spin-echo 3D sequence of the entire mouse with the following parameters: TR/TE=750/65ms and 260 mm of resolution in the three dimensions, to bring out the signal of the fat of the mice.

Gene Expression Analysis

Total RNA from cell lines was purified using RNeasy Mini Kit (QIAGEN), total RNA from murine tissues was isolated by QIAzol (QIAGEN) trituration with a motorized micropestle, followed by column purification with RNeasy Mini Kit (QIAGEN). Following the manufacturer's instructions, Superscript III Reverse Transcriptase (Invitrogen) was used with random hexamers (Promega) for generation of cDNA. Quantitative PCR was performed on a StepOnePlus Real-Time PCR System (Applied Biosystems) using TaqMan Gene Expression Master Mix (Applied Biosystems) and the following TaqMan Gene Expression Assays: murine Acbp (Mm01286585_g1), murine Pparg (Mm00440940_m1) and the murine Ppia (Mm02342430_g1) purchased by Thermo Fisher Scientific.

METHOD DETAILS

All experiments were replicated at least three times with the exception of the experiments involving human samples (that were replicated in an independent cohort) and the immunohistochemical detection of neuronal activation in mice (that was repeated once, yielding similar results). Mice were randomized into experimental groups, though without blinding of the investigators. The sample size and the statistical tests employed for each experiment are noted in the Figure Legends. There were no inclusion/exclusion criteria.

QUANTIFICATION AND STATISTICAL ANALYSIS

Data are reported as the mean ± SD, mean ± SEM, or Box and whisker plots (mean, first and third quartiles, and maximum and minimum values) as specified. Sample size and exact statistical test employed for each experiment are noted in the Figure Legends. Differences were considered statistically significant when p-values $^{\circ}p < 0.1$, $^{*}p < 0.05$, $^{**}p < 0.01$, $^{***}p < 0.001$, $^{****}p < 0.0001$ and n.s. = not significant ($p > 0.05$).

DATA AND CODE AVAILABILITY

Scans of the original western blots before cropping are available at the following URL: http://dx.doi.org/10.17632/7hdptr389m.1.